J Geophys (1985) 58:44-72

Journal of Geophysics

Gaussian beam synthetic seismograms

V. Červený
Institute of Geophysics, Charles University, Ke Karlovu 3, 12116 Praha 2, Czechoslovakia

Abstract. Numerical modelling of high-frequency seismic wave fields in complex, 2-D and 3-D, laterally varying, layered structures by the summation of elastodynamic Gaussian beams is discussed. The main attention is devoted to the expansion of the wave field into Gaussian beams, to the choice of initial parameters of Gaussian beams in these expansions and to the construction of synthetic seismograms. The Gaussian beam synthetic seismograms are regular even in regions where the ray method fails, such as the caustic region, critical region, etc. Due to the smoothing effects involved in the Gaussian beam procedure, the method is not too sensitive to the approximation of the medium and to minor details of the model. Moreover, the method does not require two-point (source-to-receiver) ray tracing. The evaluation of Gaussian beam synthetic seismograms requires approximately the same amount of computer time as the evaluation of ray synthetic seismograms. The memory requirements are also approximately the same. Numerical examples of Gaussian beam synthetic seismograms for 2-D and 3-D structures are presented. Various possible applications of Gaussian beams to seismological problem of practical importance are outlined.

Key words: Seismic waves - Synthetic seismograms - Gaussian beams

Introduction

The computation of high-frequency seismic wave fields in laterally varying, layered, two-dimensional and three-dimensional structures plays an important role in the interpretation of seismic data. The application of ray methods to this problem has been found very useful, but it has certain restrictions, see Červený (1985a). Let us mention three of these restrictions: (1) The ray method can be applied only to smooth media, in which the characteristic dimensions of inhomogeneities are considerably larger than the prevailing wavelength of the propagating wave. (2) The ray method fails in the vicinity of some surfaces, lines or points, at which the ray field is not regular (singular regions). (3) The amplitudes of high-frequency seismic waves evaluated by the ray method are very sensitive to the approximation of the medium and to minor details of the model (such as artificial interfaces of a higher order, edges in interfaces and small fictitious oscillations of the velocity function introduced by the approximation of the medium).

The first limitation is very serious and cannot be eliminated by any high-frequency asymptotic method. In this paper, we shall assume that the medium is sufficiently smooth. In order to eliminate the second restriction, various modifications of the ray method (local asymptotics) can be used. For example, let us name the Airy modification in the caustic region and the Weber-Hermite modification in the critical region. In laterally varying media, however, the structure of singular regions may be rather complicated and the singular regions often overlap. For this reason, the application of the above-named modifications becomes complicated or even impossible and is only of limited value.

Several new techniques to evaluate high-frequency body-wave synthetic seismograms have been proposed recently, which overcome partially or fully the difficulties of singular regions even in complex laterally varying structures. Let us mention the extended WKBJ method by Chapman (1978), the Maslov asymptotic theory (Chapman and Drummond, 1982; Chapman, 1985), the phase-front parabolic approximation method (Haines, 1983, 1984a, b), the Kirchhoff-Helmholtz methods (see, e.g., Sinton and Frazer, 1981, 1982; Scott and Helmberger, 1983; Frazer and Sen, 1985, where many other references can be found), the method of multifold Kirchhoff-Helmholtz path integrals (Frazer, 1983, 1985; Sen and Frazer, 1985) and the method of Gaussian beams.

In this paper, we shall mainly discuss the method based on the summation of Gaussian beams. We shall show that the method of Gaussian beams can now be used routinely to evaluate high-frequency synthetic body-wave seismograms for a broad class of realistic, laterally varying, layered, two-dimensional and three-dimensional models. It yields considerably better results in singular regions than the ray method, no matter how complicated the singularities are. Moreover, it is not so sensitive to minor details of the model as the ray method. Nevertheless, many problems in the numerical modelling of high-frequency seismic wave fields by Gaussian beams are still open to further research.

The method of Gaussian beams is a powerful gener-

alization of the ray method. It is based on the summation of Gaussian beams concentrated close to rays traced from the source (or from an initial surface). The amplitudes of Gaussian beams decrease exponentially with the square of distance from the central ray (the amplitude profile is Gaussian, i.e. bell-shaped). This is the reason why these beams are called Gaussian. The width and the curvature of the phase front of Gaussian beams change along the ray due to spreading, diffusion, reflection/transmissions and, possibly, dissipation. The final equations for Gaussian beams are valid along the whole ray, and Gaussian beams do not have any singularity at caustics.

Assume now that the receivers at which we wish to evaluate synthetic wave fields are distributed regularly or irregularly in some region D_0 along the Earth's surface or along a vertical boundary of the model (vertical seismic profiling configuration). For simplicity, we shall consider here only the receivers along the Earth's surface; there are practically no differences between the two cases from the computational point of view.

The Gaussian beam summation procedure is then as follows:

a) As in the ray method, the complete wave field is divided into elementary waves (reflected, refracted, converted, etc.).

b) For each elementary wave, initial value ray tracing or interval ray tracing (see Červený, 1985a) is performed. The endpoints of the calculated rays must cover not only the region D_0 with a sufficient density, but also some vicinity of this region. The reason for this is that a Gaussian beam concentrated close to a particular ray affects not only the wave field at the endpoint of the ray, but also the wave field in some finite vicinity of the endpoint. This may require the extension of the actual medium, if the receivers are distributed close to the side borders of the model. The problem may be simply overcome by evaluating the endpoints of rays not only along the Earth's surface, but also along the upper parts of the vertical boundaries of the model. In the whole procedure, two-point ray tracing is not required.

c) Dynamic ray tracing is then performed along the computed rays with endpoints in the region D_0 or in its vicinity. The whole fundamental matrix of the linearly independent solutions of the dynamic ray-tracing system is determined.

d) The spreading-free amplitudes are evaluated.

e) The endpoints of rays, together with the results of the dynamic ray tracing, spreading-free amplitudes and some other quantities, all specified at these endpoints, are stored in a file. The procedure is repeated for all elementary waves under consideration.

Once this file with the endpoints information for all elementary waves is available, the contributions of Gaussian beams concentrated close to individual rays can be determined at any point of the region D_0. The final synthetic wave field at a receiver situated in region D_0 is then obtained as a weighted superposition of those Gaussian beams which are situated close to the receiver. The remote Gaussian beams need not be considered in this superposition.

Note that the same file can be used to evaluate synthetic seismograms by the paraxial ray approximation approach and by some other high-frequency methods similar to the Chapman-Maslov method, etc.

In this paper, we shall discuss only the most important physical concepts of the Gaussian beam method. In most cases, we shall not present any equations; the necessary mathematical background can be found in papers listed in the references. For the most general case of three-dimensional, laterally varying, layered structures, see the detailed treatment in Červený (1985b).

Gaussian beams

There are several approaches to derive Gaussian beams. We shall describe some of them here.

The first approach is based on the application of the *parabolic wave equation method*. The fact that the high-frequency part of the seismic energy propagates mostly along rays has been well-known; see Aki and Richards (1980), p. 128. To study the waves which propagate along a certain preferred direction, it is very convenient to use the parabolic wave equation method (Leontovich and Fock, 1946; Fock, 1965). The method of the parabolic wave equation has been applied to many wave propagation problems, such as radio waves, acoustic waves and optical waves. For elastic waves, see McCoy (1977) and Hudson (1980). A detailed historical survey of various applications of the parabolic wave equation can be found in Tappert (1977). Let us mention here the applications in the research of *beam propagation* in random media, such as radars (in radio waves), sonars (in acoustic waves), lasers (in optical waves), etc. The parabolic wave equation method found very important applications even in seismic prospecting; see Landers and Claerbout (1972), Claerbout (1976), Sutton (1984). The first to use this approach to study the solutions of a wave equation concentrated close to rays was Babich (1968). See also Babich and Buldyrev (1972) and Babich and Kirpichnikova (1974). The same approach was used by Kirpichnikova (1971a) to investigate the high-frequency solutions of the elastodynamic equation concentrated close to rays of body waves. The elastodynamic equation can then be reduced to the parabolic equations for P and S waves, which further yield the dynamic ray-tracing systems and the transport equations for the amplitudes. The dynamic ray-tracing system is obtained in the form of a non-linear Riccati matrix equation, but it can simply be rewritten into any other form well-known from the ray method, see Červený (1985a, b). Contrary to the ray method, where only the real-valued solutions of the dynamic ray-tracing system are needed, the solutions concentrated at the ray require the complex-valued solutions of the dynamic ray-tracing system. The simplest solutions of the elastodynamic equation concentrated close to rays can then be identified as Gaussian beams. Higher modes correspond to Hermite-Gaussian beams, see Klimeš (1983).

For the detailed derivation of elastodynamic Gaussian beams by the parabolic wave equation method and for the discussion of their properties in 2-D and 3-D media, the reader is referred to Červený and Pšenčík (1983a, b, 1984). For elastodynamic Gaussian beams in

anisotropic media see Hanyga (1985a, b), for accoustical Gaussian beams see Babich and Popov (1981) and for scalar wave equation Gaussian beams see Červený (1981, 1982), Popov (1982), Červený et al. (1982).

The following approach to derive Gaussian beams is based on the *paraxial ray approximation*. The paraxial ray approximation can be generalized by allowing the phase function (travel time) to be complex-valued. More strictly, the travel time is real-valued along the central ray of the beam and becomes complex-valued outside the central ray. This method is used by Červený (1985b) to derive compact expressions for an arbitrary multiple reflected (possibly converted) elastodynamic Gaussian beam in a general 3-D laterally varying layered structure. The approach yields the same final equations as the parabolic wave equation method, but is more straightforward.

As the travel time is complex-valued outside the central ray of the beam, the corresponding rays in the vicinity of the central ray can be interpreted as complex rays. In this way, the Gaussian beams may be understood as *bundles of complex rays* (Keller and Streifer, 1971; Deschamps, 1971; Felsen and Marcuvitz, 1973; Felsen, 1976a). Both the positions of the points along the ray and the ray-centred components of the slowness vectors are complex-valued for complex rays. The interpretation of Gaussian beams as bundles of complex rays is closely connected with the idea of displacing a real source into a complex coordinate space (Felsen, 1976b, 1985; Ru-Shan Wu, 1985).

Alternatively, Gaussian beams can be obtained as *complex-valued solutions of the Hamilton-Jacobi and transport equations* (with a complex-valued eikonal). Such solutions were studied in great detail by Maslov and described in Maslov (1977). Maslov calls the method "the complex WKB method" and applies it to a broad variety of problems of quantum physics, propagation of narrow beams, etc. He shows that the method can also be used to solve various problems of nonlinear equations. See also Klimeš (1984b). A similar method, based on ray expansions with a complex eikonal, was used by Babich and Ulin (1981a) to find solutions of the wave equation concentrated in the neighbourhood of a closed geodesic, and by Nomofilov (1981) to find solutions of the general system of second-order differential equations concentrated close to a fixed ray. The results of Nomofilov are very general and can be applied directly to various wave fields (anisotropic elastic media, magnetic hydrodynamics, etc.). A similar method was also used by Babich and Ulin (1981b) to find concentrated wave packets (called "quasiphotons") moving along space-time rays. The method of Babich and Ulin was further modified by Katchalov (1984) who used a more suitable coordinate system centred at the space-time ray.

Here, we shall consider the 3-D Gaussian beam as the paraxial ray approximation with complex-valued travel times. The details of the evaluation of the paraxial ray approximation were explained in Červený (1985b). We shall, therefore, repeat the individual steps only very briefly.

First, we evaluate the rays. We select one ray Ω, specified by ray coordinates γ_1, γ_2, introduce the ray-centred coordinate system q_1, q_2, $q_3=s$ connected with Ω (where $q_3=s$ is the arc length along the ray Ω) and evaluate the travel time $\tau(s)$ and the relevant polarization vectors along Ω. The next step is to perform dynamic ray tracing along Ω. Dynamic ray tracing is used to evaluate the 2×2 transformation matrix $\mathbf{Q}(s)$ from ray coordinates γ_1, γ_2 to ray-centred coordinates q_1, q_2, $Q_{IJ}=[\partial q_I/\partial\gamma_J]_{q_1=q_2=0}$ (also called the matrix of geometrical spreading), and the 2×2 transformation matrix $\mathbf{P}(s)$ from ray coordinates γ_1, γ_2 to the phase space coordinates, i.e. the ray-centred components of the slowness vector $p_I=\partial\tau/\partial q_I$,

$$P_{IJ}=[\partial p_I/\partial\gamma_J]_{q_1=q_2=0}=[\partial^2\tau/\partial q_I\,\partial\gamma_J]_{q_1=q_2=0}$$

(with $I,J=1,2$). In the Gaussian beam computations, the matrices $\mathbf{Q}$ and $\mathbf{P}$ are complex-valued, whereas they are real-valued in the paraxial ray approximation. This is the most important difference of the paraxial ray approximation.

If, however, we determine the whole *fundamental matrix of real-valued linearly independent solutions* of the dynamic ray tracing system, i.e. both the plane wave and the point source solutions of the dynamic ray tracing system, any complex-valued solution of the dynamic ray tracing system can then be simply evaluated as a linear combination of the above two real-valued solutions (Červený, 1985b).

In the Gaussian beam approach, a basic role is played by the symmetric 2×2 matrix $\mathbf{M}$ of the second derivatives of the complex-valued travel time with respect to ray-centred coordinates q_1, q_2, $M_{IJ}=[\partial^2\tau/\partial q_I\,\partial q_J]_{q_1=q_2=0}$ ($I,J=1,2$), and by the 2×2 complex curvature matrix $\mathbf{K}$, $\mathbf{K}=v\mathbf{M}$, where v is the velocity. We can evaluate these matrices from $\mathbf{Q}$ and $\mathbf{P}$,

$$\mathbf{M}=v^{-1}\mathbf{K}=\mathbf{P}\mathbf{Q}^{-1}. \tag{1}$$

For Gaussian beams, we can write

$$\mathbf{M}=\operatorname{Re}\mathbf{M}+i\operatorname{Im}\mathbf{M},\qquad \operatorname{Im}\mathbf{M}>\mathbf{0}. \tag{2}$$

(By $\operatorname{Im}\mathbf{M}>\mathbf{0}$, we understand that $\operatorname{Im}\mathbf{M}$ is positive definite.) For $\operatorname{Im}\mathbf{M}=\mathbf{0}$, the Gaussian beam reduces to the paraxial ray approximation. However, if $\operatorname{Im}\mathbf{M}>\mathbf{0}$ holds at least at one point of the ray Ω, it follows that $\operatorname{Im}\mathbf{M}>\mathbf{0}$ along the whole ray Ω.

At any selected point of the ray, the matrix $\operatorname{Re}\mathbf{M}$ describes the properties of the phase front of the beam and $\operatorname{Re}\mathbf{K}$ is the curvature matrix of the phase front. Similarly, the matrix $\operatorname{Im}\mathbf{M}$ describes the width of the beam. The larger the width, the smaller $\operatorname{Im}\mathbf{M}$.

Matrix $\operatorname{Re}\mathbf{M}(s)$ fully specifies the *phase ellipse* (or phase hyperbola) which is given by the equation $\pi f[\mathbf{q}^T\operatorname{Re}\mathbf{M}(s)\mathbf{q}]=1$. Here f is the frequency and $\mathbf{q}^T=(q_1,q_2)$. Along the phase ellipse (hyperbola), the travel time is constant and differs from the travel time $\tau(s)$ on the central ray by $(\pi f)^{-1}$. Similarly, the matrix $\operatorname{Im}\mathbf{M}(s)$ specifies the *spot ellipse* which is given by the equation $\pi f[\mathbf{q}^T\operatorname{Im}\mathbf{M}(s)\mathbf{q}]=1$. The amplitude of the Gaussian beam along the spot ellipse is constant and equals $e^{-1}A(s)$, where $A(s)$ is the amplitude of the Gaussian beam at the central ray. The phase ellipse and the spot ellipse, as introduced above, are frequency dependent; they are smaller for higher frequencies. Alternatively, they can be introduced for some fixed frequency, e.g. for $f=1$ Hz.

The orientation of the phase ellipse is generally different from the orientation of the spot ellipse. Gaussian beams with a different orientation of the spot ellipse and phase ellipse are called *astigmatic Gaussian beams* (Arnaud and Kogelnik, 1969). The Gaussian beam is called the *Gaussian beam with a simple astigmatism* at $s=s_0$ if the phase ellipse and the spot ellipse have the same orientation at $s=s_0$. For the Gaussian beam which is *stigmatic (circular)* at $s=s_0$, we can write

$$\mathbf{M}(s_0)=\left[v^{-1}(s_0)\,K_0+\frac{i}{\pi L_0^2}\right]\mathbf{I}, \tag{3a}$$

where $v(s_0)$ is the velocity at $s=s_0$ and K_0 and L_0 are real constants. They determine the curvature of the phase front and the width of the circular beam at $s=s_0$, for the frequency of 1 Hz. Thus, the Gaussian beam, circular at $s=s_0$, is fully specified by two parameters, K_0 and L_0. In a laterally inhomogeneous medium, this beam immediately becomes astigmatic at $s\neq s_0$ due to inhomogeneities.

For a general astigmatic beam, the matrix $\mathbf{M}$ is specified at any point of the ray Ω by six real-valued quantities: two principal curvatures of the phase front, two principal widths of the Gaussian beam and two angles which determine the orientation of both principal directions. Thus, the system of Gaussian beams connected with any 3-D ray Ω is six-parametric.

The final expression for the displacement vector of the Gaussian beam concentrated close to the ray Ω is formally the same as the relevant expression for the displacement vector of the paraxial ray approximation (Červený, 1985a, b). The spreading-free amplitudes are identical, only the real-valued geometrical spreading is replaced by the complex-valued geometrical spreading $(\det \mathbf{Q})^{-1/2}$. Contrary to the ray solution, the expression $\det \mathbf{Q}$ does not vanish at any point of the ray in the case of Gaussian beams. The Gaussian beams are regular along the whole ray, including the caustic points.

Even in the case of Gaussian beam computations, it is again convenient to evaluate a file of *elementary wave quantities*, as in the case of the paraxial ray computation (see Červený, 1985a, b). The file contains the same quantities as in the case of the paraxial ray approximation. It must, however, contain both real-valued solutions of the dynamic ray tracing system (the whole fundamental matrix), i.e. the plane-wave solution and the point-source solution. Even if we are considering only a point source in our computation, the plane-wave solution of the dynamic ray tracing system must also be evaluated. The evaluation of the second linearly independent solution of the dynamic ray tracing system takes only a small fraction of the computer time required for the whole computation. Hence, we can say that the evaluation of the Gaussian beam requires approximately the same amount of computer time as the evaluation of the paraxial ray approximation.

In many applications, it is appropriate to use *2-D Gaussian beams*. Let us assume that the model does not depend on one Cartesian coordinate, e.g. on the coordinate x_2. Consider the rays situated in the plane $x_2=0$. We select one ray Ω. The ray is fully specified by one ray parameter, say γ (e.g. the take-off angle at the source). This parameter is the ray coordinate. The ray-centred coordinates q_i are introduced in such a way that q_2 coincides with x_2. We shall now consider Gaussian beams infinitely broad in the x_2 direction and call them 2-D Gaussian beams. All the above equations remain valid in the case of 2-D Gaussian beams, only the 2×2 matrices $\mathbf{P}$, $\mathbf{Q}$, $\mathbf{M}$, $\mathbf{K}$ are replaced by scalars P, Q, M, K, corresponding to the upper left elements of corresponding matrices. See Červený (1985b) for details. Any 2-D Gaussian beam concentrated close to Ω is then specified at any point $s=s_0$ of Ω by two real-valued quantities, $\operatorname{Re} M(s_0)$ and $\operatorname{Im} M(s_0)$. Instead of $\operatorname{Re} M(s_0)$ and $\operatorname{Im} M(s_0)$, we can again use K_0 and L_0,

$$M(s_0)=\operatorname{Re} M(s_0)+i\operatorname{Im} M(s_0)=v^{-1}(s_0)\,K_0+\frac{i}{\pi L_0^2}. \tag{3b}$$

K_0 and L_0 are the phase-front curvature and the beam-width of the 2-D Gaussian beam at $s=s_0$ in the plane $x_2=0$, for a frequency of 1 Hz. Let us again emphasize that Eq. (3b) specifies a 2-D Gaussian beam, infinitely broad in the x_2 direction, not the circular beam as in Eq. (3a).

Summation of Gaussian beams

In the Gaussian beam method, the high-frequency solution of the elastodynamic equation for any elementary wave is obtained by summation of Gaussian beams. This expansion of the high-frequency wave field into solutions concentrated close to rays was first suggested by Babich and Pankratova (1973). Asymptotic expansions of the 3-D wave field, generated by a point source, into Gaussian beams were derived by Popov (Katchalov and Popov, 1981; Popov, 1982). For the 2-D wave field generated by a line source, see Červený et al. (1982) and Müller (1984). For the expansion of a plane wave into Gaussian beams, see Červený (1981, 1982).

A more general approach to derive the expansion equations of a high-frequency wave field into Gaussian beams was used by Klimeš (1984a), who applied the approach to a scalar 3-D wave field given on an arbitrary smooth initial surface. A similar approach was applied to a vectorial 3-D wave field by Červený (1985b), where various asymptotic expansions for an arbitrary multiple reflected (P, S or converted) elementary wave are derived. We shall present, without derivation, one of these general expansions. The expansion is applicable to different types of wave fields: for the wave field generated by a point or line source, for the wave field specified at an initial surface of arbitrary shape, at some wavefront, at the Earth's surface, at an exploding reflector, etc.

We denote the displacement vector of an elementary wave, evaluated at any point S by the Gaussian beam method, by $\hat{\mathbf{u}}^G(S)$. The general expansion formula can then be written in the following form:

$$\hat{\mathbf{u}}^G(S)=\iint_D \Phi^N(\gamma_I)\,\hat{\mathbf{U}}^N(O_s)\exp\left[i\omega\tau(S,O_s)\right]d^2\gamma. \tag{4}$$

Here γ_1, γ_2 are the ray parameters, e.g. the take-off angles in the case of a point source or the curvilinear coordinates along the initial surface. The integration is

over the ray parameters and ω is the circular frequency. Each set of ray parameters γ_1, γ_2 specifies one central ray and relevant Gaussian beam concentrated close to this ray. Point O_s is the orthogonal projection of the point S on to the ray specified by the ray parameters γ_1, γ_2. $\hat{\mathbf{U}}^N(O_s)$ is the vectorial complex-valued spreading-free amplitude at the point O_s, $\tau(S, O_s)$ is the Gaussian beam complex-valued travel time at S. In ray-centred coordinates,

$$\tau(S, O_s)=\tau(O_s)+\tfrac{1}{2}\mathbf{q}^T\mathbf{M}(O_s)\mathbf{q}, \tag{5}$$

where $\mathbf{q}^T=(q_1, q_2)$, q_1 and q_2 being the ray-centred coordinates of point S. The weighting function Φ^N is given by the relation,

$$\Phi^N(\gamma_I)=\frac{\omega}{2\pi}\,|\det\mathbf{Q}^{\mathbf{R}}(O_s)|^{1/2} \cdot\{-\det[\mathbf{M}(O_s)-\mathbf{M}^{\mathbf{R}}(O_s)]\}^{1/2}, \tag{6}$$

with

$$\mathrm{Re}\{-\det[\mathbf{M}(O_s)-\mathbf{M}^{\mathbf{R}}(O_s)]\}^{1/2}>0. \tag{7}$$

In Eqs. (5)–(7), the quantity $\tau(O_s)$ denotes the real-valued travel time at O_s, evaluated along the ray specified by ray coordinates γ_1, γ_2. $\mathbf{M}(O_s)$ is the complex-valued matrix of the second derivatives of the complex travel time, corresponding to the Gaussian beam concentrated close to ray γ_1, γ_2.

Matrix $\mathbf{M}(O_s)$ is influenced by the choice of initial parameters of Gaussian beams used in the evaluation of Eq. (4). Matrices $\mathbf{M}^{\mathbf{R}}(O_s)$ and $\mathbf{Q}^{\mathbf{R}}(O_s)$ have similar meaning to $\mathbf{M}(O_s)$ and $\mathbf{Q}(O_s)$ and are again evaluated along the ray γ_1, γ_2. They are, however, real-valued and characterize the paraxial ray approximation of the ray field under consideration, not a Gaussian beam. For a given ray field (e.g. corresponding to a point source), $\mathbf{M}^{\mathbf{R}}(O_s)$ and $\mathbf{Q}^{\mathbf{R}}(O_s)$ are fully specified at any point O_s of the ray γ_1, γ_2. They are not influenced by the choice of initial parameters of Gaussian beams used in the expansion (4).

The evaluation of all quantities in expansion (4) is easy. The only numerical problem consists in the evaluation of points O_s, i.e. the orthogonal projections of S on to the individual rays. This step would require all computed rays to be stored. Expansion (4), however, remains valid even if O_s is not the projection of S on to ray Ω, but if O_s is an arbitrary point on Ω, situated close to S. The only equation which must be slightly modified in this case is the equation for $\tau(S, O_s)$. For details, see Červený (1985a, b). Note that the coordinates of points O_s and S may be specified in Cartesian coordinates in the final expansion integrals. In most of these computations, we consider points O_s to be *the endpoints of rays* along the Earth's surface.

The expansion equation, Eq. (4), was derived using Gaussian beams. Strictly speaking, however, it is not an expansion into Gaussian beams. The complex-valued geometrical spreading factor from the expression for Gaussian beams was introduced into the expression for the weighting function, where it was cancelled with some other factors. For simplicity, we shall continue to refer to Eq. (4) as the expansion into Gaussian beams.

In two-dimensional computations, we obtain,

$$\hat{\mathbf{u}}^G(S)=\int_D \Phi^N(\gamma)\,\hat{\mathbf{U}}^N(O_s)\,L_\perp^{-\frac{1}{2}}(O_s)\exp[i\omega\tau(S, O_s)]\,d\gamma. \tag{8}$$

Here γ is the ray parameter, $\hat{\mathbf{U}}^N(O_s)$ is the spreading-free amplitude which is practically the same as in the 3-D case (it may differ from it only by some source factors, taken at O_s). Function $\tau(S, O_s)$ can also be evaluated in a standard way. Function $L_\perp(O_s)$ is the transverse spreading. For a line source, $L_\perp(O_s)=1$; for a point source $L_\perp(O_s)=\int_{O_0}^{O_s} v(s)\,ds/v(O_0)$, where the integral is taken along the ray from the source O_0 to the endpoint O_s. These expressions for $L_\perp(O_s)$ follow from general equations for more complicated situations, derived by Červený (1985b). $\Phi^N(\gamma)$ again denotes the weighting function, given by the following relation,

$$\Phi^N(\gamma)=\left(\frac{\omega}{2\pi}\right)^{1/2}|Q^R(O_s)|^{1/2} \cdot\{-i[M(O_s)-M^R(O_s)]\}^{1/2}, \tag{9}$$

with

$$\mathrm{Re}\{-i[M(O_s)-M^R(O_s)]\}^{1/2}>0. \tag{10}$$

The quantities M, M^R and Q^R are the scalar equivalents of matrices $\mathbf{M}$, $\mathbf{M}^{\mathbf{R}}$ and $\mathbf{Q}^{\mathbf{R}}$.

Let us emphasize one important point regarding the asymptotic expansions in Eqs. (4) and (8). They are applicable to any orthonomic system of rays, whatever the source of the wave field. The properties of the actual ray field under consideration are hidden in matrices $\mathbf{Q}^{\mathbf{R}}(O_s)$, $\mathbf{M}^{\mathbf{R}}(O_s)$, and in the spreading-free vectorial amplitude $\hat{\mathbf{U}}^N(O_s)$. For example, for a point source, $\hat{\mathbf{U}}^N(O_s)$ contains the radiation pattern of the source.

Discrete expansions

If the integrands of the expansion integrals in Eqs. (4) and (8) are sufficiently smooth for given S and ω, the integrals may be evaluated by numerical quadratures. In this way, we obtain the discrete expansion of the wave field into Gaussian beams. The wave field at the receiver point S is obtained as a weighted superposition of contributions, corresponding to individual beams passing in the neighbourhood of the receiver. The Gaussian beams corresponding to remote rays have no substantial effect on the result at the point S and need not be considered.

The discretization error was investigated by Klimeš (1985). The relative average quadratic error $\delta(\Sigma)$ over some region Σ caused by the discretization of Eqs. (4) or (8), may be defined by the following formula:

$$\delta(\Sigma)=\{\int_\Sigma |\hat{\mathbf{u}}^G(S)-\hat{\mathbf{u}}^{GD}(S)|^2\,d\Sigma/\int_\Sigma |\hat{\mathbf{u}}^G(S)|^2\,d\Sigma\}^{1/2},$$

where $\hat{\mathbf{u}}^G(S)$ is given by Eq. (4) or (8), $\hat{\mathbf{u}}^{GD}(S)$ denotes the discrete version of $\hat{\mathbf{u}}^G(S)$. To be brief, we shall consider only the 2-D expansion, Eq. (8). The error $\delta(\Sigma)$ is closely connected with the real-valued non-negative

quantities $\kappa^2(O_s)$,

$$\kappa^2(O_s)=\pi f(\Delta\gamma)^2[Q^R(O_s)]^2 \cdot \{[\mathrm{Re}\,M(O_s)-M^R(O_s)]^2[\mathrm{Im}\,M(O_s)]^{-1} + \mathrm{Im}\,M(O_s)\}, \quad O_s\in\Sigma, \tag{11}$$

where $\Delta\gamma$ is the discretization step in the ray parameter γ, f is the frequency and the other quantities have the same meaning as in Eq. (9). Generally, the error $\delta(\Sigma)$ is greater for greater values of κ^2. For κ^2 fixed, the error is a minimum if the quantities $\Delta\gamma$, Q^R, M^R, M, $\hat{\mathbf{U}}^N$, $L_\perp$ are approximately constant over Σ and is greater if these quantities vary considerably from beam to beam. We shall present the relations between the error $\delta(\Sigma)$ and κ^2 given by Eq. (11) in two extreme canonical cases, see Klimeš (1985):

a) The regular case. The quantities $\Delta\gamma$, Q^R, M^R, M, $\hat{\mathbf{U}}^N$, $L_\perp$ are assumed to be constant for all beams and $\Sigma\to(-\infty,\infty)$. Then $\delta(\Sigma)=\delta^{\mathrm{REG}}(\Sigma)$, where

$$\delta^{\mathrm{REG}}(\Sigma)=\sqrt{2}\exp(-\pi^2\kappa^{-2}).$$

We may also define the relative maximum error in this case:

$$\delta^{\mathrm{REG}}_{\mathrm{MAX}}(\Sigma)=\underset{S\in\Sigma}{\mathrm{Max}}\{|\hat{\mathbf{u}}^G(S)-\hat{\mathbf{u}}^{GD}(S)|/|\hat{\mathbf{u}}^G(S)|\}.$$

Then we obtain

$$\delta^{\mathrm{REG}}_{\mathrm{MAX}}(\Sigma)=2\exp(-\pi^2\kappa^{-2}).$$

b) The irregular case. The amplitude $\hat{\mathbf{U}}^N$ is constant and non-zero only in the elementary interval of the size of the discretization step $\Delta\gamma$ and zero outside it. Such a case simulates a region with sharp changes of amplitudes, e.g. the boundary between the shadow and illuminated zones. The relative average quadratic error may, under some conditions, be approximately evaluated. It is, of course, considerably larger than $\delta^{\mathrm{REG}}(\Sigma)$ and is given by the relation

$$\delta^{\mathrm{IRREG}}(\Sigma)=\kappa^2/(4\sqrt{3}).$$

In practical computations, it may be useful to keep the quantity $\kappa^2(O_s)$ fixed, or at least under some limit. For a given $\kappa^2(O_s)$, the error lies roughly between $\delta^{\mathrm{REG}}(\Sigma)$ and $\delta^{\mathrm{IRREG}}(\Sigma)$.

For κ^2 fixed, relation (11) offers very useful possibilities to control certain important quantities, e.g. $\Delta\gamma$ or $\mathrm{Im}\,M(O_s)$:

1) If the frequency f and the quantities Q^R, M^R, $\mathrm{Re}\,M$ and $\mathrm{Im}\,M$ are given, Eq. (11) may be used to evaluate $\Delta\gamma$. This possibility represents some sort of interval ray tracing, in which the discretization step $\Delta\gamma$ is automatically determined from the local parameters of the ray field at the endpoints O_s of the ray $[Q^R(O_s)$ and $M^R(O_s)]$ and from the properties of Gaussian beams at $O_s[\mathrm{Re}\,M(O_s)$ and $\mathrm{Im}\,M(O_s)]$.

2) If $\Delta\gamma$, f, Q^R, M^R and $\mathrm{Re}\,M(O_s)$ are given or properly chosen, Eq. (11) may be used to evaluate $\mathrm{Im}\,M(O_s)$. See Eq. (17).

3) $\mathrm{Im}\,M(O_s)$ may be also determined from Eq. (11) by minimizing $\kappa^2(O_s)$, i.e. by minimizing the discretization error. See Eq. (14).

There are also several other possibilities of how to exploit relation (11).

For 3-D media, all the expressions are similar to those presented above, but the scalars must be replaced by matrices. For other details, see Klimeš (1985).

Gaussian beam synthetic seismograms

The time-domain equivalents of Gaussian beams are wave packets; see Babich and Ulin (1981b), Červený (1983). Wave packets propagate along rays and are firmly tied to them. If the source-time function is given by the Gaussian envelope (Gabor) signal,

$$F(t)=\exp\{-[2\pi f_M(t-t_0)/\gamma]^2\} \cdot \cos[2\pi f_M(t-t_0)+\nu], \tag{12}$$

where f_M, t_0, γ and ν are some real-valued parameters, the wave packets have a Gaussian envelope both in time and space. These packets are then called *Gaussian packets* (or Gaussian envelope packets). Similarly, if the source-time function is the Dirac delta function, the wave packets are called *delta packets*. The detailed expressions for wave packets are given in Červený (1983, 1985b).

As with ray synthetic seismograms, Gaussian beam synthetic seismograms can be evaluated by three approaches: (a) by direct summation of wave packets, (b) by the frequency-domain approach and (c) by the convolutory approach.

In the first approach, based on the summation of wave packets, two summations must be performed: the first summation is over elementary waves and the second over the wave packets forming the elementary wave. Only wave packets which propagate along the rays situated in the vicinity of the receiver need to be considered. The wave packets propagating along remote rays need not be considered. Nevertheless, the number of wave packets in the Gaussian beam approach is considerably larger than the number of elementary seismograms in the ray synthetic seismogram evaluation. For this reason, the first approach is usually more time consuming than the frequency-domain approach, where we can again use the fast method to evaluate the frequency response (see Červený, 1985a). The convolutory approach, supplemented by some smoothing procedures, is very useful and efficient in the case of the summation of paraxial ray approximations, with real-valued travel times (see Chapman, 1985). It seems that the approach is not so efficient in the Gaussian beam approach, where the complex-valued travel times must be considered. The subject is, however, open for further research.

Choice of initial parameters of Gaussian beams in the expansion

There is some degree of freedom in the expansion formulae, Eqs. (4) and (8), as the parameters of Gaussian beams used in the expansion [represented by matrix $\mathbf{M}(O_s)$] may, to some extent, be chosen arbitrarily. Moreover, they can be specified at different points of the rays, as dynamic ray tracing can be used to recalculate $\mathbf{M}$ from one point of the ray to another.

The most straightforward way is to choose **M** directly at the endpoint O_s of the ray. Equations (4) and (8) can then be used directly. Another possibility is to specify **M** at the source (or at the initial surface). In this case, we must recalculate $\mathbf{M}(O_0)$ to $\mathbf{M}(O_s)$, using the fundamental matrix of linearly independent solutions of the dynamic ray tracing system. We can also specify **M** at any other point Q of the ray, e.g. at a point of reflection/transmission at an interface. Again, $\mathbf{M}(Q)$ must be recalculated to $\mathbf{M}(O_s)$ using the fundamental matrix. The possibility of specifying **M** at an interface is very promising for certain applications.

We shall now discuss the problem of choosing matrix **M**. In 3-D computations, we have six free real-valued parameters at our disposal. In regular ray regions, the expansion integrals yield the ray solution. The value of the integral does practically not depend on the choice of $\mathbf{M}(O_s)$ in this case. The behaviour of the asymptotic expansions (4) and (8) in singular-ray regions is, however, more complicated. The value of the integrals there depends on the choice of the initial parameters of Gaussian beams.

The freedom in the choice of the initial parameters of Gaussian beams not only has certain advantages but also disadvantages. The advantage consists mainly in the generality of the presented expansion formulae. Many of the presently available high-frequency modifications of the ray method are in fact special cases of these expansions. These special cases may be very convenient in some situations, e.g. for roughly vertically inhomogeneous media, but may fail in some other situations. On the contrary, the Gaussian beam method may be adapted to various situations merely by the proper choice of the initial parameters. The disadvantage is that the optimum choice of the initial parameters (which would yield results of the highest accuracy) is not yet fully known.

The proper choice of the initial parameters of Gaussian beams in the expansion equations has been investigated mostly by numerical comparisons with more accurate or exact solutions (reflectivity, finite differences, integral equations, etc.), or by the application of the reciprocity principle. In practically all computations, considerably better results were obtained by the summation of Gaussian beams than by the ray method. Several useful recommendations regarding the choice of $\mathbf{M}(O_s)$ have been made. It was found that for media which are roughly one-dimensional (only vertically inhomogeneous, radially symmetric) and in which the velocity changes only smoothly, the most accurate results are obtained with broad Gaussian beams. In this case, the Gaussian beam method yields results almost identical to the results obtained with some other methods, which use $\mathrm{Im}\,\mathbf{M}=\mathbf{0}$ (extended WKBJ, Maslov method). The computations with Gaussian beams, however, are more stable and suppress various spurious arrivals typical of the case of $\mathrm{Im}\,\mathbf{M}=\mathbf{0}$. They do not fail at p-caustics. Moreover, the number of rays needed in the expansion may be considerably smaller than in the case of $\mathrm{Im}\,\mathbf{M}=\mathbf{0}$. See the example in the next section.

As soon as some more pronounced lateral variations appear in the medium, the choice of very broad Gaussian beams is not the best. The Gaussian beam method, however, may still be able to handle such situations. As an example, we shall consider the waves reflected from an interface with an edge. In principle, the Gaussian beam summation method can then not be applied. Nevertheless, it was shown both analytically and numerically that the results are satisfactorily accurate if the Gaussian beams used in the expansion are rather narrow in the vicinity of the edge. For details, see numerical example 5. A similar conclusion is valid even for other conspicuous inhomogeneities on which the Gaussian beams must be "focused".

The *optimum choice* of matrix **M** in the expansion equations, which would minimize the error, is now the subject of investigations. It is obvious that such a choice will depend on the whole history of each ray and on the velocity distribution in the immediate vicinity of the ray (mainly on the velocity gradients).

The optimum choice of $\mathrm{Re}\,\mathbf{M}$ and $\mathrm{Im}\,\mathbf{M}$ will be shortly discussed at the end of this section. Here, however, we shall describe a *very stable choice*, which can be used quite automatically. We assume that the receivers are distributed along the Earth's surface and that the file containing all necessary quantities at the endpoints of rays along the Earth's surface is available. We shall specify $\mathrm{Re}\,\mathbf{M}$ and $\mathrm{Im}\,\mathbf{M}$ at the endpoint O_s of the central ray of the beam. We consider models with a curved Earth's surface and with velocity gradients (both vertical and horizontal) varying along the Earth's surface.

A) *Choice of* $\mathrm{Re}\,\mathbf{M}$

It is very convenient to choose $\mathrm{Re}\,\mathbf{M}(O_s)$ in such a way as to obtain zero second derivatives of the travel-time field along the Earth's surface Σ in the vicinity of the endpoint O_s. This will remove some oscillatory functions from the expansion integrals and will yield more stable results. This choice yields Gaussian beams with *effective plane phase fronts* (not with actual plane phase fronts!). We shall call this choice the *effective plane phase front choice;* its mathematical form is as follows:

$$\mathrm{Re}\,\mathbf{M}(O_s)=-\mathbf{G}^{-1}[v^{-1}\cos\vartheta\,\mathbf{D}+\mathbf{E}](\mathbf{G}^T)^{-1}. \tag{13}$$

Here ϑ is the "angle of incidence", $0\leqq\vartheta\leqq\pi$, i.e. the angle between the vector tangent to the incident ray and the normal to Σ at O_s, $v=v(O_s)$ is the velocity of the incident wave at O_s. Matrix **D** denotes the 2×2 curvature matrix of Σ at O_s. **G** is the 2×2 upper left corner submatrix of the 3×3 transformation matrix from ray-centred (q_i) to the local Cartesian coordinate system (z_i) at Σ at O_s, with z_3 measured along the normal to Σ. Finally, **E** is a 2×2 matrix which specifies the velocity gradients in the vicinity of O_s. If the medium is homogeneous at O_s, then $\mathbf{E}=\mathbf{0}$, the null matrix. The symbol T denotes the transpose. More details and precise specification of the individual matrices can be found in Červený (1985b). If the effective plane phase front choice, Eq. (13), is applied, the actual phase front of the Gaussian beam under consideration is generally curved at O_s. Only if a plane Earth's surface ($\mathbf{D}=\mathbf{0}$), overlying a homogeneous layer ($\mathbf{E}=\mathbf{0}$), is involved, the effective plane phase front choice yields the true plane phase front of the Gaussian beam [$\mathrm{Re}\,\mathbf{M}(O_s)=\mathbf{0}$].

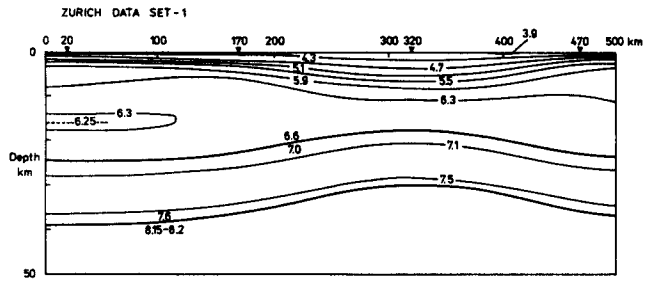

Fig. 1. The 2-D laterally varying Earth's crust model Zurich, used for the computation of several numerical examples in this paper. The *bold lines* denote interfaces, the *thin lines* the isolines of velocity. The shot points (SP) are situated at $x=20$ km, $x=170$ km, $x=320$ km and $x=470$ km

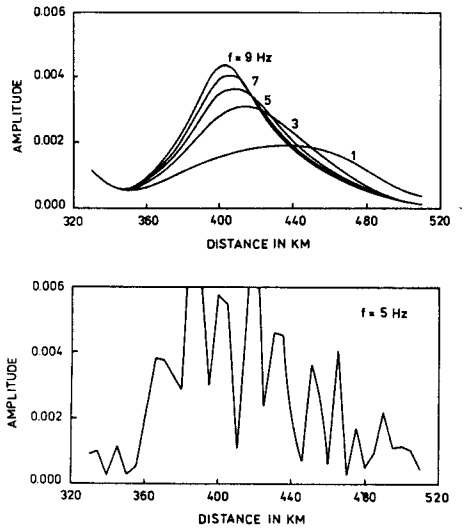

Fig. 2. Amplitude-distance curves of the *PP* wave reflected from the intermediate crustal interface in the model Zurich, SP=320 km (see Fig. 1) computed by the summation of Gaussian beams. The vertical component of the displacement vector is considered. The numbers marking the curves denote frequencies (in Hz). In the *top diagram*, the effective plane phase front option, Eq. (13), for $\mathrm{Re}\,M(O_s)$ was used. The *bottom diagram* corresponds to plane phase fronts [$\mathrm{Re}\,M(O_s)=0$ s/km^2]. In both cases, $\mathrm{Im}\,M(O_s)=0.001$ s/km^2, i.e. $L_0=17.8$ km

To demonstrate the application of the above option, we shall use the 2-D laterally varying Earth's crust model Zurich, described in detail in Červený (1985a). The model is shown in Fig. 1. The interfaces are shown as bold lines, the thin lines correspond to the isolines of velocity. Note that the gradients of velocity (both vertical and horizontal) are rather high and vary considerably along the Earth's surface. We shall not investigate here whether the validity conditions are fulfilled in our computations, we are just interested in whether our Gaussian beam algorithm yields stable results, even for regions with larger velocity gradients. We shall consider the shot point SP=320 km. In Fig. 2, the amplitude-distance curves for the vertical component of the wave reflected from the intermediate crustal interface are shown. In the upper part, the effective plane phase front choice, Eq. (13), for $\mathrm{Re}\,M(O_s)$ was applied. (As the computations are two-dimensional, $M(O_s)$ is not a matrix but a scalar.) The amplitude-distance curves correspond to five frequencies, $f=1, 3, 5, 7, 9$ Hz. The maxima of the amplitude-distance curves are shifted beyond the critical point which is situated at $x=385$ km. The smaller the frequency, the larger the shift. The lower picture shows the amplitude-distance curve for the same wave and frequency $f=5$ Hz, evaluated with the choice $\mathrm{Re}\,M(O_s)=0$, i.e. with the actual plane phase fronts at the endpoints of rays. As we can see, the curve is very unstable. Note that $\mathrm{Im}\,M(O_s)$ was taken to be constant, equal to 0.001 s/km^2, i.e. $L_0=17.8$ km.

The effective plane phase front choice (13) for $\mathrm{Re}\,\mathbf{M}$ may also be used in a slightly modified form at the source. This choice then yields the WKBJ initial conditions, discussed in detail by Madariaga (1984).

B) *Choice of* $\mathrm{Im}\,\mathbf{M}$

This choice specifies the width of Gaussian beams. For $\mathrm{Im}\,\mathbf{M}=\mathbf{0}$, there is no Gaussian windowing. In laterally inhomogeneous layered structures, Gaussian windowing is always useful (although small windowing is often sufficient) as it increases the stability of the computations considerably.

Very stable results have been obtained by the option which minimizes the discretization error, caused by replacing the continuous expansion into Gaussian beams by a discrete expansion, see Eq. (11). In 3-D media, it can be expressed as follows:

$$\mathrm{Im}\,\mathbf{M}(O_s)=\{[\mathbf{M}^{\mathbf{R}}(O_s)-\mathrm{Re}\,\mathbf{M}(O_s)]^2\}^{1/2}. \tag{14}$$

In Eq. (14), the square root of a positive-definite symmetric matrix $\mathbf{A}=(\mathbf{M}^{\mathbf{R}}-\mathrm{Re}\,\mathbf{M})^2$ is a positive definite symmetric matrix $\mathbf{B}$ such that $\mathbf{BB}=\mathbf{A}$.

We shall generalize this option slightly,

$$\mathrm{Im}\,\mathbf{M}(O_s)=C\{[\mathbf{M}^{\mathbf{R}}(O_s)-\mathrm{Re}\,\mathbf{M}(O_s)]^2\}^{1/2}, \tag{15}$$

where C is a positive constant close to 1.

Note that option (15) has a very interesting property. If Eq. (15) is valid at the endpoint O_s of the ray Ω, we obtain, under certain conditions specified in Červený (1985b), the following relation:

$$\tan \int_{O_0}^{O_s} v\,\mathrm{tr}\,[\mathrm{Im}\,\mathbf{M}(s)]\,ds=2C(1-C^2)^{-1}. \tag{16}$$

Here $\mathrm{tr}\,[\mathrm{Im}\,\mathbf{M}(s)]$ denotes the trace of matrix $\mathrm{Im}\,\mathbf{M}(s)$ and the integral in Eq. (16) is taken along the ray Ω. The integral is small for Gaussian beams which are globally broad (between points O_0 and O_s) and large for Gaussian beams which are globally narrow. Thus, condition (15) yields globally narrow Gaussian beams for short rays and globally broad Gaussian beams for long rays. The most stable results are obtained if C is close to 1.

Option (15) leads to stable results, even if it is applied to refracted waves evaluated both in the immediate vicinity of the source and at larger epicentral distances. If we chose $\mathrm{Im}\,\mathbf{M}=\mathrm{const.}$, the strong wave field of the refracted wave close to the source would influence the whole section and would yield very strong spurious arrivals. For those elementary waves which all

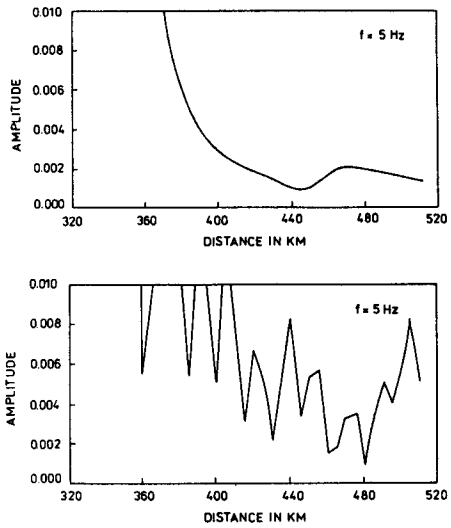

Fig. 3. Amplitude-distance curves of the P refracted wave in the first layer for model Zurich, SP = 320 km (see Fig. 1) computed by the summation of Gaussian beams. A frequency of 5 Hz is considered. In the *top diagram*, $\mathrm{Im}\, M(O_s)$ is selected according to Eq. (14); in the *bottom diagram*, $\mathrm{Im}\, M(O_s)$ is constant and equal to 0.001 s/km^2 ($L_0 = 17.8$ km). In both cases, $\mathrm{Re}\, M(O_s)$ is determined from Eq. (13)

have rays of approximately the same length, option (15) is, of course, not so critical; $\mathrm{Im}\,\mathbf{M}$ may be taken constant. This applies, e.g., to all elementary reflected waves from deeper interfaces, see Fig. 2.

Let us present an example. In Fig. 3, the amplitude-distance curves of the *wave refracted* in the first layer in 2-D model Zurich, SP = 320 km, are presented. The upper picture corresponds to option (14), the lower option is computed with constant $\mathrm{Im}\, M = 0.001$ s/km^2, i.e. $L_0 = 17.8$ km. (Again, M is a scalar quantity, as the computations are two-dimensional.) The strong wave field close to the source contaminates the weak wave field at large distances in the second case. The choice of constant $\mathrm{Im}\, M$ then yields unstable results. Both curves correspond to a frequency of 5 Hz. The effective plane phase front choice was used to determine $\mathrm{Re}\, M(O_s)$.

In some situations, it may happen that $\mathbf{M}^R(O_s) - \mathrm{Re}\,\mathbf{M}(O_s)$ vanishes. In this case, option (15) would yield $\mathrm{Im}\,\mathbf{M}(O_s) = 0$, which does not represent a Gaussian beam. But some Gaussian windowing is always useful. For this reason, it is suitable to modify Eq. (15) in the following way:

$$\mathrm{Im}\,\mathbf{M}(O_s) = C\{[\mathbf{M}^R(O_s) - \mathrm{Re}\,\mathbf{M}(O_s)]^2 + \mathbf{A}_{\min}^2\}^{1/2}. \qquad (15')$$

Here $\mathbf{A}_{\min}$ is some optional real-valued symmetric positive-definite matrix, which specifies the lower bound of $\mathrm{Im}\,\mathbf{M}(O_s)$. (It may also be useful to consider an upper bound for $\mathrm{Im}\,\mathbf{M}(O_s)$ in Eq. (15'), as $\mathbf{M}^R(O_s)$ is infinite at caustic points.)

Generally, the above choice of $\mathrm{Im}\,\mathbf{M}(O_s)$ yields very stable results. It is, however, not the optimum choice in the sense of minimizing the error of computations, but it offers a useful compromise. For roughly vertically inhomogeneous media, more accurate results are usually obtained with lower $\mathrm{Im}\,\mathbf{M}(O_s)$ (broader Gaussian beams) than suggested above. In this case it may be useful to choose the Gaussian beams as broad as possible, but so that κ^2, given by Eq. (11), related to the discretization error, does not exceed some limit. For simplicity, we shall again present the final result only for 2-D computations. In the case of regular initial-value ray tracing with the step $\Delta\gamma$ we obtain approximately from Eq. (11),

$$\mathrm{Im}\, M(O_s) = \pi\kappa^{-2} f(\Delta\gamma)^2 (Q^R)^2 (\mathrm{Re}\, M - M^R)^2. \qquad (17)$$

The meaning of individual symbols is the same as in Eq. (11).

Option (17) leads to very accurate results in a smooth medium without conspicuous lateral variations. Even in media with lateral variations, however, it usually yields useful results, but it often generates spurious arrivals.

Using the integral expansions, Eqs. (4) or (8), we can also evaluate *ray synthetic seismograms* by the summation of very narrow Gaussian beams. If we wish to evaluate ray synthetic seismograms, we must choose $\mathrm{Re}\,\mathbf{M}(O_s) = \mathbf{M}^R(O_s)$, and $\mathrm{Im}\,\mathbf{M}(O_s)$ very large. In the case of 2-D computations and regular initial-value ray tracing with a step $\Delta\gamma$, Eq. (11) again yields approximately

$$\mathrm{Im}\, M(O_s) = \kappa^2 [\pi f (\Delta\gamma)^2 (Q^R)^2]^{-1}. \qquad (18)$$

For a more detailed explanation and a numerical example, see Červený (1985a).

At the end of this section, we shall add several notes to the optimum choice of $\mathrm{Re}\,\mathbf{M}(O_s)$ and $\mathrm{Im}\,\mathbf{M}(O_s)$ which would minimize the error of computations. Before we study this error, it is useful to formulate *the validity conditions for Gaussian beams.* The validity conditions may be formulated in various ways. We shall write here three such validity conditions; two of them are for smooth media without interfaces and the third applies to the interaction of the Gaussian beam with an interface. Limited space does not allow us to give the exact formulation and a detailed discussion of these conditions here. For a detailed treatment, see Klimeš (1985); other publications are under preparation.

The *first validity condition* requires that the complex curvature of the wavefront of the beam be small over the spot ellipse. In other words, the components of the slowness vector perpendicular to the central ray must be small over the spot ellipse. The condition can be expressed as

$$(v^2/2\pi f)\,\mathrm{tr}\,[\mathbf{M}(\mathrm{Im}\,\mathbf{M})^{-1}\mathbf{M}^+] \ll 1,$$

where $\mathbf{M}^+$ is the Hermite adjoint matrix to $\mathbf{M}$.

The *second validity condition* restricts the variations of the slowness over the spot ellipse. Alternatively, it restricts the variations of the norm of the slowness vector over the spot ellipse. The condition may be written as follows:

$$(1/2\pi f v^2)\,\mathbf{Z}^T(\mathrm{Im}\,\mathbf{M})^{-1}\mathbf{Z} \ll 1,$$

where $\mathbf{Z}^T = (\partial v/\partial q_1, \partial v/\partial q_2)$.

The *third validity condition* applies to the interaction of the Gaussian beam with the interface. It requires that the second derivatives of the complex-valued travel

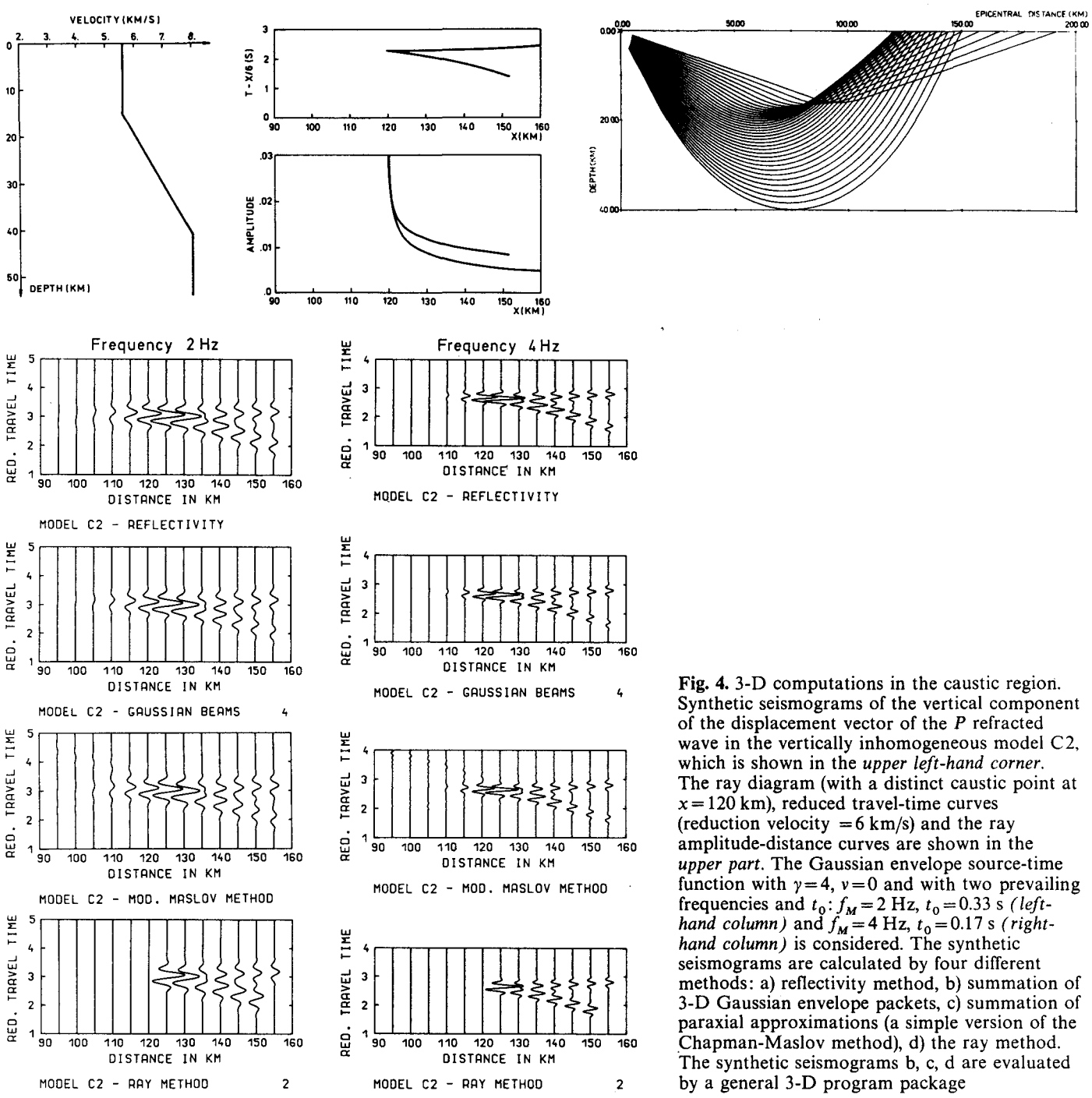

Fig. 4. 3-D computations in the caustic region. Synthetic seismograms of the vertical component of the displacement vector of the P refracted wave in the vertically inhomogeneous model C2, which is shown in the *upper left-hand corner.* The ray diagram (with a distinct caustic point at $x = 120$ km), reduced travel-time curves (reduction velocity $= 6$ km/s) and the ray amplitude-distance curves are shown in the *upper part.* The Gaussian envelope source-time function with $\gamma = 4$, $\nu = 0$ and with two prevailing frequencies and t_0: $f_M = 2$ Hz, $t_0 = 0.33$ s *(left-hand column)* and $f_M = 4$ Hz, $t_0 = 0.17$ s *(right-hand column)* is considered. The synthetic seismograms are calculated by four different methods: a) reflectivity method, b) summation of 3-D Gaussian envelope packets, c) summation of paraxial approximations (a simple version of the Chapman-Maslov method), d) the ray method. The synthetic seismograms b, c, d are evaluated by a general 3-D program package

time of the beam along the interface be small over the spot ellipse. The condition can be expressed as follows

$$(v^2/2\pi f)\,\mathbf{e}^T(\mathbf{M}-\mathbf{M}^E)(\mathrm{Im}\,\mathbf{M})^{-1}(\mathbf{M}-\mathbf{M}^E)\,\mathbf{e} \ll 1.$$

Here $\mathbf{M}^E$ is the right-hand side of Eq. (13), $\mathbf{e}^T = (e_1, e_2)$, where e_i are components of the unit vector tangent to the interface in a plane of incidence into the q_i axes of the ray-centred coordinate system.

As we can see, the first validity condition requires broad Gaussian beams; the second, narrow Gaussian beams. The second condition is especially severe for regions with larger velocity gradients, where rather narrow Gaussian beams must be used to satisfy the condition.

The *optimum choice* can then be obtained by minimizing the relevant expressions in the validity conditions along the central ray of the beam. Certain minimizing equations of this type were obtained by Klimeš (1985). They yield the optimum values of $\mathrm{Re}\,\mathbf{M}(O_s)$ and $\mathrm{Im}\,\mathbf{M}(O_s)$ as a result. They are now the subject of practical testing.

For a detailed treatment of various validity conditions and for relevant numerical examples, see also Ben-Menahem and Beydoun (1985a, b).

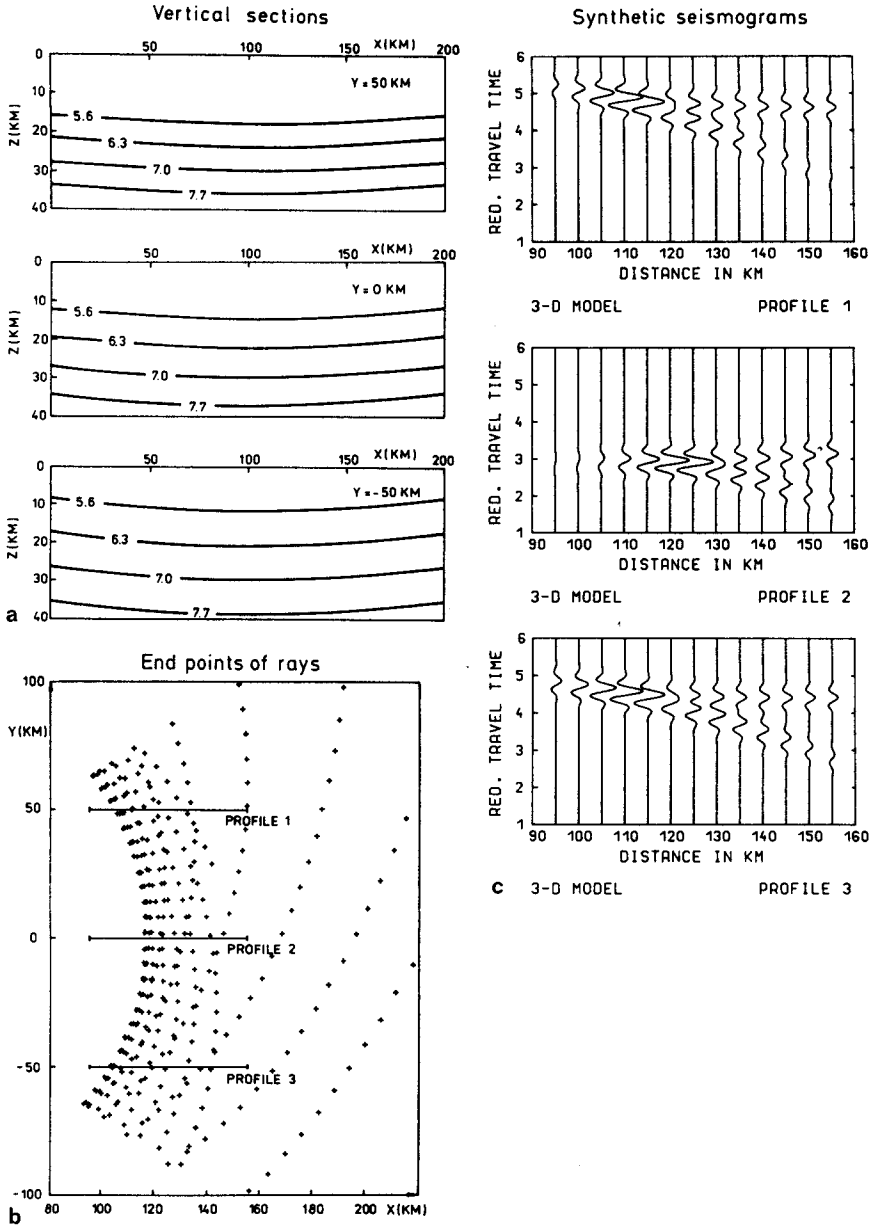

Fig. 5. 3-D computations in the caustic region. Synthetic seismograms of the vertical component of the displacement vector of the *P* refracted wave in the 3-D model, which is shown in the *upper left-hand part* of the figure. The 3-D model is demonstrated here by the isolines of velocity in three vertical sections corresponding to planes $y=50$ km, $y=0$ km and $y=-50$ km. The source is situated at $x=y=z=0$ km. The map of endpoints of 3-D rays along the Earth's surface used in the evaluation of synthetic seismograms is shown in the *bottom diagram.* The Gaussian envelope source-time function with $\gamma=4$, $\nu=0$, $t_0=0.33$ s and $f_M=2$ Hz is considered. The synthetic seismograms are computed by the summation of 3-D Gaussian envelope packets, the receivers are distributed along profiles 1, 2, 3 shown in the map of endpoints. The time axis is reduced with respect to the x-coordinate (not with respect to the epicentral distance), the reduction velocity being 6 km/s

Numerical example 1.
Vertically inhomogeneous model C2

In this section, we shall investigate the accuracy of the Gaussian beam method in comparison with the reflectivity method. We shall use a simple 1-D model C2, see Fig. 4, in which the refracted wave forms a caustic. The point source of *P* waves with an isotropic radiation pattern is situated at the origin of the Cartesian coordinates. The source-time function has the form of the Gaussian envelope signal, Eq. (12), with $\gamma=4$, $\nu=1.57$, f_M (the prevailing frequency) equals 2 Hz or 4 Hz, $t_0=\frac{3}{2}f_M^{-1}$.

From the ray diagram we can see that the caustic is formed at $x=120$ km at the surface of the Earth. The reduced travel-time curve has two branches beyond the caustic, whereas a shadow zone is formed in front of the caustic. The next shadow zone is formed at $x>152$ km in the first (lower) branch of the refracted wave. The diagram of ray amplitudes shows the well-known behaviour of ray amplitudes in the vicinity of the caustic, with infinite amplitudes exactly at the caustic.

Synthetic seismograms evaluated by four different methods are shown in Fig. 4, for the prevailing frequencies of 2 Hz (left-hand-side column) and 4 Hz (right-hand-side column). The travel-time axes are reduced, the reduction velocity is 6 km/s. The first diagram in each column was evaluated by the reflectivity method and the last by the ray method. The synthetic seismograms calculated by the reflectivity method clearly show the differences with respect to ray synthetic seismograms. The wave field penetrates into the geometrical shadow in front of the caustic. The maximum amplitudes occur at some distance beyond the caustic, not exactly at the caustic. The wavelets in the two branches do not have the same form; the phase shift of $\frac{1}{2}\pi$ is clearly observed. The lower branch of the re-

fracted wave penetrates even into the geometrical shadow zone beyond $x=152$ km.

The second diagram in each column was evaluated by the Gaussian beam method, by the summation of 3-D Gaussian envelope packets. The *3-D program BD83* was used for this computation. In the simple model under consideration, the choice of initial parameters of Gaussian beams is not too critical. The initial parameters of Gaussian beams were chosen at the source. Circular Gaussian beams were used, see Eq. (3a), with $K_0=0$ km^{-1} and $L_0=16$ km the same for all beams. The total number of 3-D Gaussian beams used in the computation was 130. In the next diagram (denoted mod. Maslov method), paraxial ray approximations (with $\mathrm{Im}\,\mathbf{M}=\mathbf{0}$) were used instead of Gaussian beams in the summation. As we can see, the general behaviour of the wave field computed by the Gaussian beam method is very similar to that obtained by the reflectivity method. The wave field penetrates into both shadow zones and the maximum amplitudes are shifted beyond the caustic. The amplitudes do not differ by more than 11 per cent. Due to the summation of infinitely wide Gaussian beams (paraxial ray approximations) in the third diagram of each column, the number of rays used in the computation had to be increased about seven times (to 884), in comparison with the second diagram to obtain stable results. If the number of rays was smaller, the picture was covered by noisy oscillations. Even with the large number of rays used, a spurious arrival can be seen in the diagrams.

Thus, we can see that even slight Gaussian windowing increases the stability and effectiveness of computations considerably, in comparison with the paraxial ray approximation summation. The windowing also largely removes the spurious arrivals. For more details on this example, see Červený and Klimeš (1984).

Numerical example 2. Simple 3-D model

The program package BD83 used to evaluate numerical example 1 in the previous section can, of course, be used in synthetic seismogram computations for actual 3-D models. A simple 3-D modification of the model C2 is used in this numerical example, see Fig. 5. The synthetic seismograms were evaluated by the summation of 3-D Gaussian envelope packets. As the upper part of the model is again homogeneous, various simple choices of initial parameters of Gaussian beams can be used, practically without any difference to the results. In the example, stigmatic Gaussian beams with $K_0=0$ km^{-1}, $L_0=15$ km at the source were used, the source is situated at $x=y=z=0$ km. The total number of beams used in the computation was 330. For more details on this example, see Červený and Klimeš (1984).

Figure 5 demonstrates the possibility of performing 3-D computations of synthetic seismograms by the Gaussian beam method. These 3-D Gaussian beam computations are, in principle, no more time consuming than the ray computations. In all following examples, we shall consider 2-D models.

Numerical example 3. Critical region

In this section, we shall apply the Gaussian beam method to the computation of *PP* waves reflected from a plane interface between two homogeneous media, see Fig. 6. We shall concentrate our attention on the critical region and on head waves. To see the results more clearly, we shall present computations in the frequency domain. We consider the point source and the receivers situated 30 km above the interface, in the upper halfspace with the *P*-velocity 6.4 km/s. The *P*-velocity in the lower half-space is 8 km/s. In both halfspaces, $v_s=v_p/\sqrt{3}$, $\rho=1$ g/cm^3. The amplitude-distance curves are shown in Fig. 7, for a frequency of 6.4 Hz. In the top diagram, we can see the amplitude-distance curve of the *PP* reflected wave computed by exact methods (bold solid line), in comparison with some ray computations. In the bottom diagram, the exact amplitude-distance curve is compared with the Gaussian beam calculation. The exact amplitude-distance curve was computed by integration along a special contour in the complex plane, see the description of the method in Červený (1967). Both methods give practically identical results, not only in the subcritical "regular" region, but also in the critical region and at overcritical distances. In the critical region, where the ray theory fails, the Gaussian

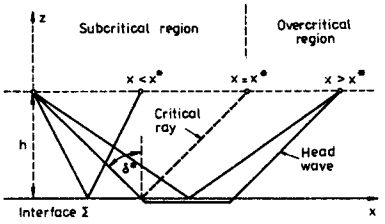

Fig. 6. Critical region. Simple model of a plane interface between two homogeneous media with *P*-velocity 6.4 km/s (upper half-space) and 8 km/s (lower half-space). Rays of several elementary waves are shown. In the overcritical region, head waves are also generated

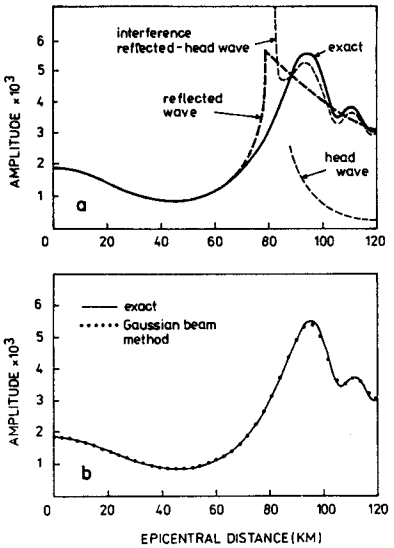

Fig. 7. Critical region. *Top:* Amplitude-distance curve of *PP* reflected wave in the model shown in Fig. 6, computed by the exact method *(bold line)*, in comparison with ray computations. *Bottom:* the same, but in comparison with Gaussian beam computations *(dots)*. The frequency is 6.4 Hz, Gaussian beam parameters chosen at the source are $K_0=0$ km^{-1}, $L_0=71.5$ km

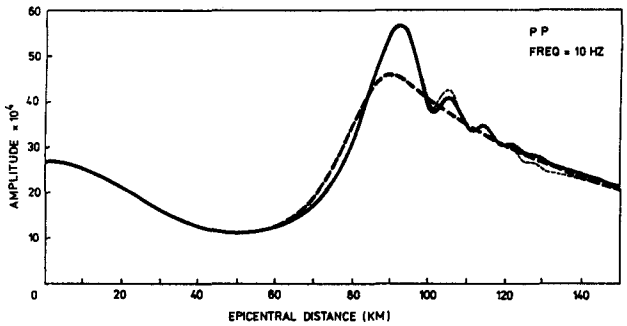

Fig. 8. Critical region. Amplitude-distance curves of *PP* refracted wave for the model shown in Fig. 6, computed by the summation of Gaussian beams. The Gaussian beam parameters are specified at the interface, $K_0=0$ km^{-1}. The *bold solid line* corresponds to very broad Gaussian beams ($L_0=100$ km) and the *bold dashed line* to very narrow Gaussian beams ($L_0=14$ km). The *thin dashed line* corresponds again to narrow Gaussian beams ($L_0=14$ km), with the exception of a very narrow vicinity of the critical point where L_0 increases smoothly from 14 km to 100 km at the critical point

beam method correctly predicts the shift of the maximum of the amplitude-distance curve beyond the critical point. At overcritical distances, the amplitude-distance curve oscillates due to the existence of head waves. Thus, the head waves are included in the superposition of the reflected Gaussian beams. In the computations, the parameters of Gaussian beams were specified at the source, with $K_0=0$ km^{-1}, $L_0\sim 70$ km, the same for all beams. The number of rays was 200.

The problem of head waves is, however, more complicated. Pure head waves are more sensitive to the choice of the initial parameters of Gaussian beams than the reflected wave field itself. Head waves are obtained only if the width of Gaussian beams is rather large. If the width is smaller, the overcritical amplitudes are smoothed. The smoothing practically does not change the general form of the amplitude-distance curves of the reflected wave, but may remove, to some extent or completely, the oscillations of the amplitude-distance curve at overcritical distances. In other words, the smaller widths usually lead to some decrease of the amplitudes of head waves. An example is shown in Fig. 8, for a frequency of 10 Hz. The model is practically the same as in Fig. 7, only the densities are evaluated from v_P using the relation $\rho=1.7+0.2\,v_P$. For all three amplitude-distance curves in Fig. 8, the initial parameters of Gaussian beams were specified at the interface with $K_0=0$ km^{-1}. The bold solid line was evaluated for $L_0\sim 100$ km and gives the exact solution. The bold dashed line corresponds to very narrow Gaussian beams, with $L_0=14$ km. The total number of rays used in the computation was 200. The smoothing effect at overcritical distances is obvious. The head waves are fully removed. The third, thin dashed line, shows the possibility of increasing the accuracy of computations by "focusing" Gaussian beams on certain singular regions. The width was chosen to be generally very small, $L_0=14$ km, with the exception of a very narrow vicinity of the critical point, where L_0 increased smoothly from 14 km to the maximum value of 100 km at the critical point. The width of this vicinity of the critical point was about 10 km. Even though the Gaussian beams remain generally very narrow (with the exception of the critical region), the increase in the accuracy of computations is tremendous. The curve practically coincides with the exact solution, with the exception of small deviations in two regions.

The example confirms the possibility of focusing Gaussian beams on certain regions of interest (singularities, conspicuous inhomogeneities, edges in interfaces, etc.). Whereas broad Gaussian beams must be used in critical regions, certain other singularities require very narrow Gaussian beams.

The diagrams presented in this section were computed by single-purpose programs written for the detailed investigation of properties of reflected and transmitted wave fields (*PP*, *PS*, *SP*, *SS*), generated at a plane interface. For details and many other computations see Konopásková and Červený (1984) and Černohlávková (1985).

Let us add one interesting point. The Gaussian beam method correctly predicts even certain *non-ray effects*. For example, it gives non-vanishing normal incidence amplitudes of converted *PS* waves (horizontal component) and converted *SP* waves (vertical component). These normal incidence amplitudes of converted waves are very stable, they practically do not depend on the choice of initial parameters of Gaussian beams.

Numerical example 4. Irregularities in interfaces

The Gaussian beam method, strictly speaking, can not be applied to the evaluation of synthetic seismograms of waves reflected from interfaces with corners, edges, etc. It would, however, be very interesting to see the behaviour of Gaussian beam synthetic seismograms in such situations and to compare them with the ray synthetic seismograms.

Figure 9 shows three simple examples. In each example, the source-to-receiver ray diagrams, ray synthetic seismogram sections and Gaussian beam synthetic seismogram sections are shown. The rays in the Gaussian beam synthetic seismogram computations were evaluated by initial-value ray tracing, the number of rays was 200. Even a considerably smaller number of rays, however, would be sufficient to obtain stable results. The initial parameters of Gaussian beams were specified at the source in all cases, $K_0=0$ km^{-1}, $L_0=25$ km for all beams under consideration. The reduction velocity is 7 km/s. No amplitude scaling is used; true amplitudes are plotted. The velocities above and below the interface are again 6.4 km/s and 8 km/s, as in the previous example. The source is situated at $x=200$ km, close to the Earth's surface. Program package BEAM 81, described in Červený (1983), was used for the Gaussian beam computations. The synthetic seismograms in BEAM 81 are evaluated as a superposition of Gaussian envelope packets, with $\gamma=4$, $\nu=0$, $f_M=4$ Hz, $t_0=0$ s.

The diagrams clearly show the differences between the ray synthetic seismograms and the Gaussian beam synthetic seismograms. We shall add only several short notes.

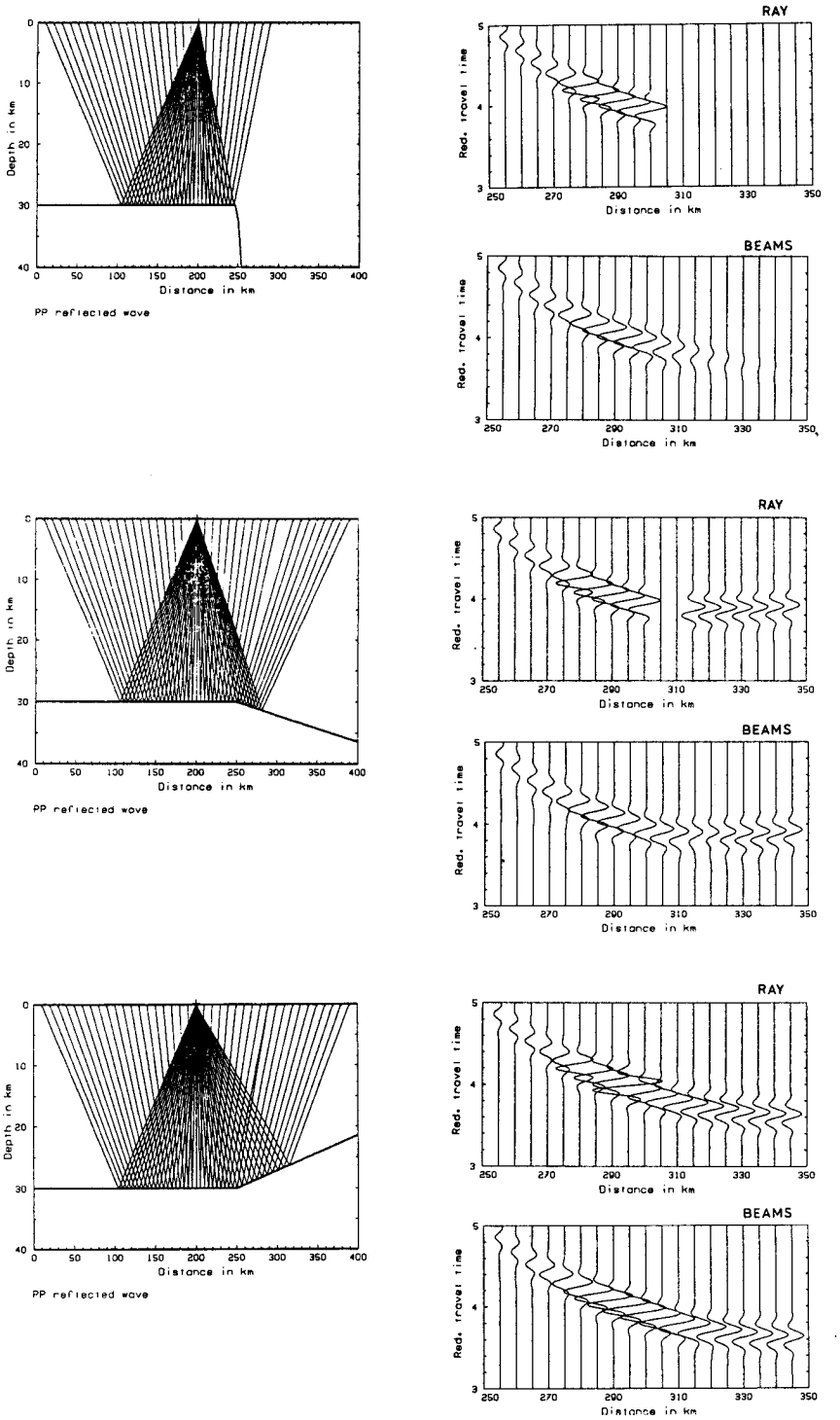

Fig. 9. Interface with a corner. Comparison of ray synthetic seismograms of *PP* waves reflected from the interface with the synthetic seismograms obtained by the summation of Gaussian envelope packets. The Gaussian envelope source-time function, with $\gamma=4$, $\nu=0$, $t_0=0$ s and $f_M=4$ Hz is considered. The time axis is reduced, the reduction velocity being 7 km/s. Three examples are considered, see the *left-hand side* of the figure, where the source-to-receiver ray diagrams are shown. The relevant ray synthetic seismograms and Gaussian envelope packets synthetic seismograms are shown on the *right-hand side*. The parameters of Gaussian beams specified at the source are $K_0=0$ km^{-1}, $L_0=25$ km

In the first diagram, we can see a model of a simple block structure. The ray method yields a sharp boundary between the illuminated and shadow zone. The Gaussian wave packets, however, give a smooth transition in this region. Some energy penetrates even into the shadow zone. The amplitudes decrease with increasing distance from the boundary to the shadow zone.

The second model contains a corner in the interface.

Due to the corner, a small shadow zone is formed close to $x=305$–310 km. The Gaussian beams give a smooth wave field in this region.

The third ray diagram corresponds to another model with a corner point at the interface. The ray diagram shows two branches of rays with a short overlapping region close to $x=295$ km. Due to the overlapping, the ray amplitudes are approximately doubled at $x=295$ km. The Gaussian beam envelope packets give smooth synthetic seismograms close to $x=295$ km. (The amplitudes are, of course, higher in this region, but smooth).

The presented synthetic seismograms do not contain head waves. The reason is as follows. In the ray synthetic seismogram computations, the pure head waves are evaluated independently of the reflected waves. In the program SEIS 81, used to evaluate ray synthetic seismograms, the pure head waves are not considered. In the Gaussian beam computations, the head waves are contained in the reflected wave field. To obtain them, Gaussian beams with a large width must be used, see numerical example 3. In this section, however, L_0 is not chosen large enough.

More details on the presented examples can be found in Červený (1983). See also the next example.

Numerical example 5. Rigid half-screen

Katchalov et al. (1983) computed the wave field in the vicinity of the edgepoint of a rigid half-screen by the summation of Gaussian beams and compared it with the exact solutions. The calculations were performed in a 2-D homogeneous medium with a rigid half-screen, in the frequency domain. An incident plane wave was considered. The angle of incidence was 45°. The exact solution was evaluated using Fresnel integrals, see Hönl et al. (1961).

The method of summation of Gaussian beams yields results qualitatively close to exact solutions if Gaussian beams, which are narrow in the vicinity of the edge, are used.

One example is shown in Fig. 10. (The author is indebted to I. Pšenčík for the results of the original computations from which Fig. 10 was drawn.) The incident plane wave was expanded into 2-D Gaussian beams with the same parameters along the wavefront. The parameters K_0 and L_0 were specified formally along the wavefront going through the edge. The choice of K_0 and L_0 along that wavefront was as follows: $K_0=0$ km^{-1}, $L_0=1$ km. This means that the width of the Gaussian beams used has a minimum along the wavefront running through the edge. In Fig. 10, the distribution of amplitudes of the wavefield along a circle with its centre at the edgepoint and with the radius 2λ is shown (λ... wavelength). The bold line shows the exact solution, the dashed line the Gaussian beam solution. The solution includes both the incident and reflected wave. The mutual interference of both waves generates typical lobes. The comparison is satisfactory, with the exception of one lobe where the Gaussian beam amplitudes are about 25% less.

The results obtained by the Gaussian beam summation method can be improved if a cylindrical diffracted wave generated at the edgepoint of the half-screen is evaluated and added to the result. A central ray field (with its centre at the edge) corresponds to this diffracted wave. The diffracted wave field is expanded into Gaussian beams concentrated close to rays of the central ray field, as in the case of the wave field generated by a line source. The weighting function in the integral expansion is found by comparison with the exact solution. For other details see Katchalov et al. (1983). The wave field which also includes the diffracted wave is shown by a dot-dashed line in Fig. 10.

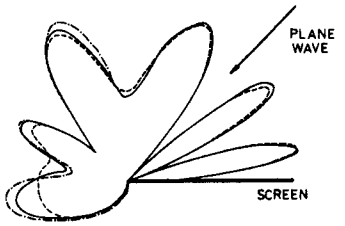

Fig. 10. The plane acoustic harmonic wave incident on a rigid half-screen. Propagation velocity in the model is 5 km/s, $f=10$ Hz, angle of incidence is 45°. The parameters of Gaussian beams, chosen along the wavefront going through the edge, are $K_0=0$ km^{-1} and $L_0=1$ km. The amplitudes of the complete wave field (incident + reflected) along a circle with its centre at the edgepoint and with a radius of 2λ ($=1$ km) are shown. The *bold line* corresponds to the exact solution, the *dashed line* is obtained by the summation of Gaussian beams. The *dot-dashed* line also includes a diffracted wave generated at the edgepoint of the half-screen

Numerical example 6. Smoothing effect of Gaussian beams

In this example, we show the smoothing effect of the Gaussian beam summation method. Whereas the ray method is very sensitive to minor details in the approximation of the medium, the Gaussian beam method is more robust and stable. To see the results more clearly, we shall present the computations in the frequency domain (not synthetic seismograms).

We shall consider a vertically inhomogeneous medium. A fast and efficient program package for the computation of Gaussian beam synthetic seismograms in general vertically inhomogeneous layered structures, called VEGA, was written by Janský and Červený. The package is a simple modification of the relevant program package for the evaluation of ray synthetic seismograms, described in detail by Červený and Janský (1985a). The velocity distribution between two grid points is specified by the law $z=z(v)$ instead of $v=v(z)$, particularly by the cubic polynomial in v^{-2}, $z=a_i+b_i v^{-2}+c_i v^{-4}+d_i v^{-6}$. Here, z denotes the depth and v the velocity. At those depths where the velocity varies smoothly and monotonically with depth (no interfaces of first-order), the coefficients a_i, b_i, c_i, d_i may be calculated by the smoothed cubic spline approximation. The approximation then guarantees the continuity of the velocity-depth distribution with its first and second derivatives at grid points. We shall call this approximation *the smoothed spline approximation.*

Alternatively, we can specify the velocity-depth distribution between two grid points just by the linear polynomial in v^{-2}, $z=a_i+b_i v^{-2}$. The approximation

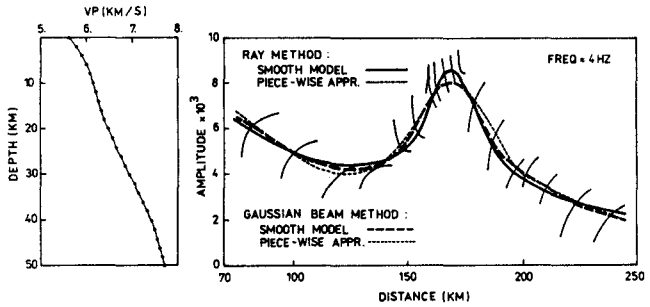

Fig. 11. The amplitude-distance curves of the *P* refracted wave in the vertically inhomogeneous model shown on the *left-hand side* of the figure. The velocity-depth distribution is approximated in two ways: by the smoothed spline approximation and by the piece-wise interpolation. The piece-wise interpolation introduces fictitious interfaces of second-order. The amplitude-distance curves are evaluated by the ray method and by the Gaussian beam method. The ray calculations are considerably influenced by the approximation method, mainly by the fictitious interfaces of second-order. The Gaussian beam method is not so sensitive to the approximation method; the results are reliable even for the piece-wise approximation

does not guarantee the continuity of velocity derivatives and introduces artificial interfaces of second-order at each grid point. We shall call it *the piece-wise approximation.*

For both these approximations the ray integrals can be simply evaluated analytically. The evaluation requires only the computation of one square root and of some polynomial for each "layer" between two grid points. No transcendental functions are required. In this way the evaluation of ray integrals is very fast and is not much slower than for a system of homogeneous layers.

The most efficient approach would be to use just the piece-wise approximation. The ray method, however, is very sensitive to the interfaces of second-order, generated by the piece-wise approximation. This is not the case with Gaussian beams, which may be safely used even in the case of the piece-wise approximation.

An example is shown in Fig. 11. The velocity is specified at depths $0, 2, \ldots, 50$ km, see Fig. 11. The two approximations described above are used to simulate the velocity-depth distribution. The differences between these two approximations are very small and are not visible in the graph.

In spite of this, the differences between the amplitude-distance curves of the vertical component of the refracted *P* waves for both approximations, evaluated by the ray method, are tremendous. The amplitude-distance curve for the smoothed spline approximation is quite stable and smooth. On the contrary, the piece-wise approximation yields quite unstable results. Any artificial interface of the second-order exerts a great effect on the amplitude-distance curve, causing anomalous behaviour of amplitudes (zeros, infinities, discontinuities). The resulting amplitude-distance curve is a tangle of short steep discontinuous segments and does not even enable us to follow the actual trend of amplitudes.

The behaviour of the amplitude-distance curves evaluated by the Gaussian beam method is quite different. They are smooth and stable for both approximations. The differences between the results for the two approximations are not large, see Fig. 11. Thus, the Gaussian beam method is not sensitive to the artificial interfaces of second-order and may be safely applied even to the case of the piece-wise approximation. This is the large advantage of Gaussian beams in comparison with the ray method.

Let us add that the parameters of Gaussian beams in this example were specified at endpoints of rays, $K_0 = 0$ km^{-1}, $L_0 = 9$ km. The number of rays evaluated by the standard initial-value ray tracing was close to 350. The example is taken from Červený and Janský (1985b).

Numerical example 7. Model Zurich

In this section, we shall present examples of Gaussian beam computations for a more realistic 2-D laterally varying layered model of the Earth's crust. We shall again use model Zurich, see Fig. 1, and consider a point source of *P* waves situated at $SP = 320$ km, close to the Earth's surface. In synthetic seismogram computations, we shall consider the *P* refracted waves in the first, second and third layers and the *PP* reflected waves from the intermediate interface and from the Mohorovičić discontinuity. Model Zurich was discussed in detail in Červený (1985a). For a better orientation in the synthetic seismogram sections, the travel-time curves of all *P* waves under consideration are shown in Fig. 12. The arrows indicate the position of relevant critical points.

The examples presented in this section and in the following two sections were evaluated by *the program package BEAM 84.* Program package BEAM 84 is similar to the program package SEIS 83, which is described in Červený (1985a). The routines for the approximation of the model, generation of numerical codes of elementary waves, radiation patterns, spreading free amplitudes, etc., are exactly the same in both packages.

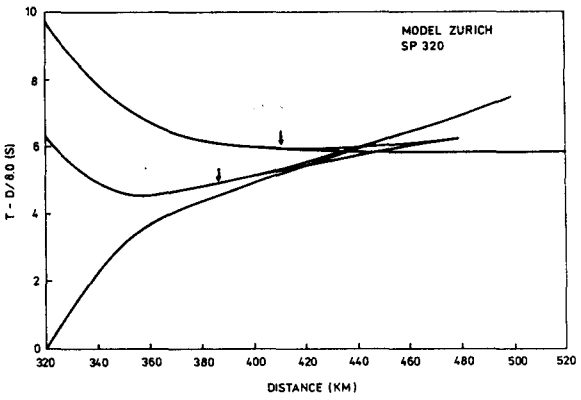

Fig. 12. Model Zurich. Reduced travel-time curves of *P* waves used in the synthetic seismogram computations in numerical examples 7, 8 and 9 (Figs. 14, 15b, 16, 19–22). The point source is situated at SP = 320 km. The travel-time curves correspond to the *P* refracted waves in the first, second and third layer and to the *PP* reflected waves from the intermediate crustal interface and from the Mohorovičić discontinuity. The reduction velocity is 8 km/s

Program package BEAM 84 consists of five programs. The first, basic program, is also called BEAM 84; the others are called GBSYN, SYNT, BPLOT and RAYPLOT.

In the first program, initial-value or interval ray tracing and dynamic ray tracing are performed and the spreading-free amplitudes are evaluated. The whole fundamental matrix of linearly independent solutions is computed. Various results of computations at all endpoints of rays along the Earth's surface are stored in the final file.

As soon as this file is available, the evaluation of Gaussian beam synthetic seismograms in any system of receivers situated along the Earth's surface is easy. The frequency-domain approach is used to evaluate synthetic seismograms. In the program GBSYN, this file is used to evaluate the frequency response in a specified system of receivers. The position of receivers and the initial parameters of Gaussian beams are specified only in GBSYN. The radiation patterns, the absorption mechanism and some frequency-dependent effects are also evaluated in GBSYN.

Thus, it is simple to recalculate the results several times with different parameters of Gaussian beams, different radiation patterns, absorption mechanism, receiver positions, etc. Frequency-dependent amplitude-distance curves can be constructed, see the examples in Figs. 2 and 3. Also paraxial ray approximations (infinitely broad Gaussian beams) can be used in computations. Ray, WKBJ and Maslov computations may be performed by the proper choice of initial parameters of Gaussian beams.

The next program, *program SYNT*, evaluates synthetic seismograms from the frequency response for arbitrary high-frequency source-time functions. Detailed pictures of frequency responses, spectra of synthetic seismograms and synthetic seismograms at any receiver can be plotted. See the examples in Figs. 13 and 23.

Finally, *program BPLOT* is used to plot synthetic seismogram sections. Similarly, *program RAYPLOT* can be used to plot the ray diagrams, the travel-times and the spreading-free amplitudes.

Let us now return to model Zurich. We shall again use the Gaussian envelope signal, with $f_M = 5$ Hz, $\gamma = 4$, $\nu = 0$, $t_0 = 0.4$ s. The signal and its amplitude spectrum are shown in Fig. 13. The spectrum was windowed to remove frequencies less than 1 Hz and higher than 10 Hz. This windowing practically does not change the signal, see Fig. 13, and considerably increases the effectivity of computations. Moreover, very low frequencies must be removed to satisfy the validity conditions of the Gaussian beam method. However, whether the validity conditions listed earlier were fulfilled in our computations or not was not investigated quantitatively.

Due to stronger velocity gradients along the Earth's surface, the initial parameters of Gaussian beams were chosen at the endpoints of rays in the way recommended earlier. More specifically, the effective plane phase front option (13) was used to determine $\mathrm{Re}\, M$, and Eq. (15) to determine $\mathrm{Im}\, M$. The rays were evaluated by interval ray tracing, with the length of the interval 2 km. This means that at least one ray endpoint of each elementary wave is available in any illuminated region of the length 2 km along the profile.

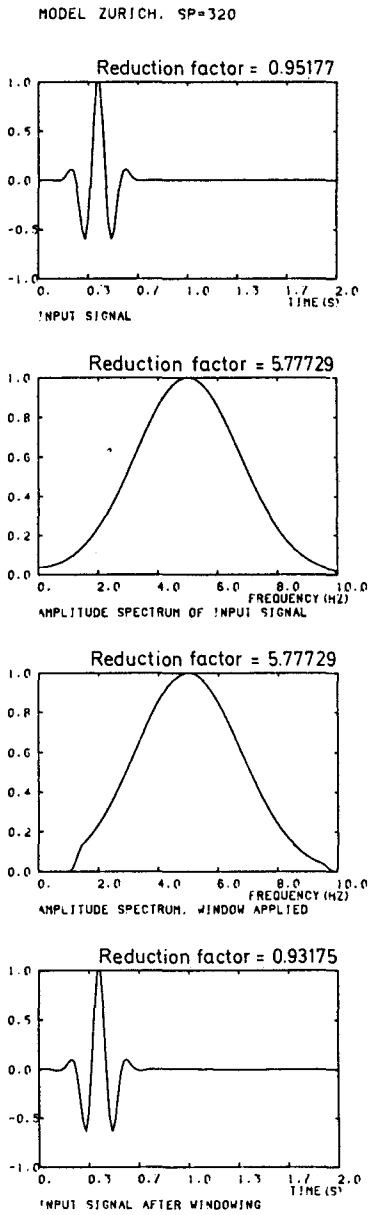

Fig. 13. The Gaussian envelope source-time function ($\gamma = 4$, $\nu = 0$, $t_0 = 0.4$ s, $f_M = 5$ Hz) used in the next synthetic seismogram computations. The amplitude spectrum, windowed amplitude spectrum and the signal after spectral windowing are shown

The constant C in Eq. (15) was varied to show the differences. With the exception of very low C, stable results were obtained. Figure 14 shows the synthetic seismogram sections for five different constants C: 5, 2, 1, 0.5, 0.2. The reduction velocity is 8 km/s. Power scaling of amplitudes is used; the trace at the epicentral distance r is multiplied by the factor $35\ (r/20)^1$. Here r is measured in kilometres and amplitude $= 1$ corresponds to the plotting distance between two neighbourhood traces in the plots of the synthetic seismogram sections.

If we compare the Gaussian beam synthetic seismograms with the travel-time curves, see Fig. 12, and with the ray synthetic seismograms, see Fig. 9a in Červený (1985a), we can observe some expected differences.

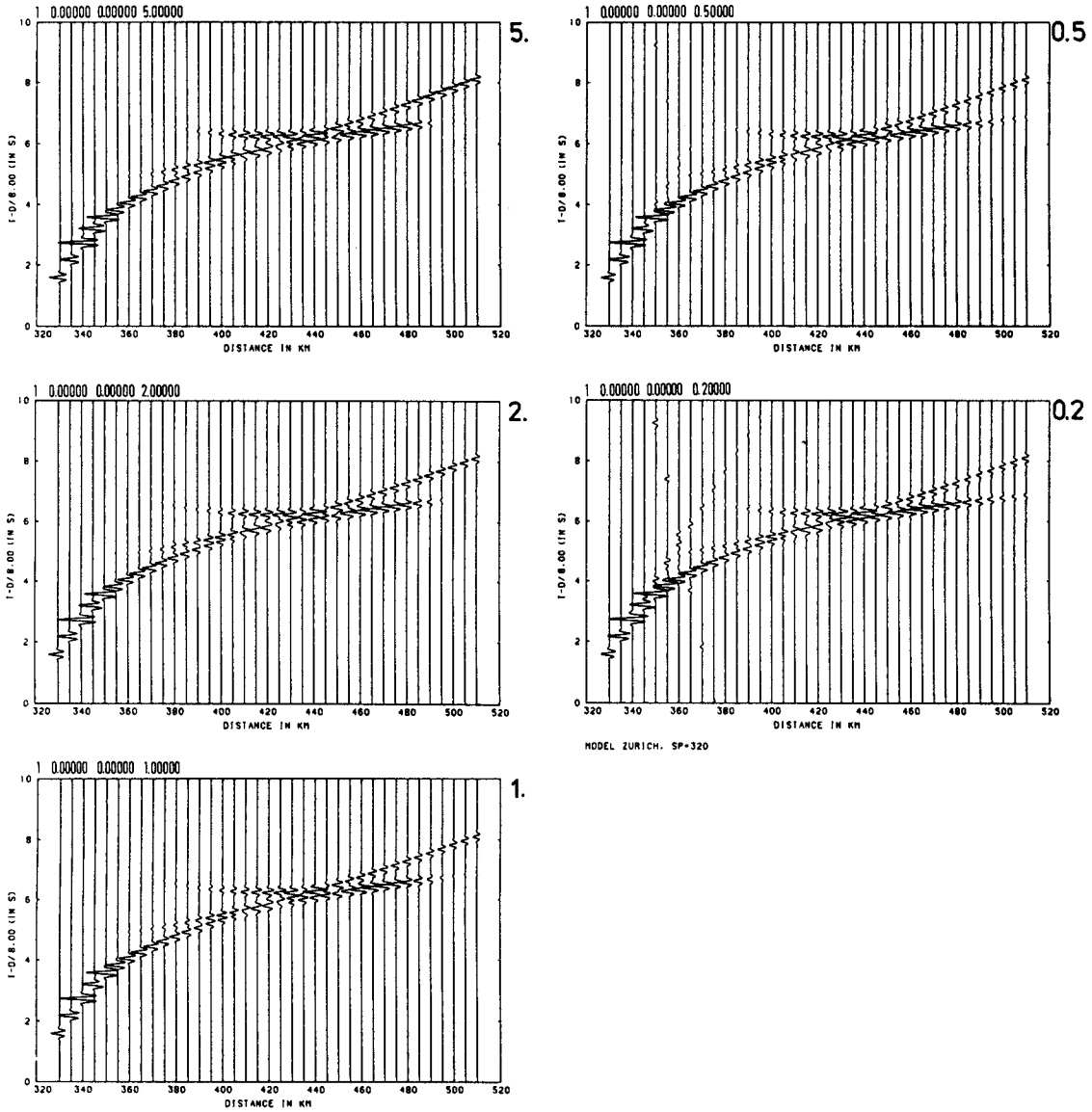

Fig. 14. Choice of parameters of Gaussian beams. Gaussian beam synthetic seismograms of the vertical component of the displacement vector in the model Zurich, SP = 320 km (see Fig. 1). The parameters of Gaussian beams are chosen at the endpoints of rays, using Eq. (13) to determine Re $M(O_s)$ and Eq. (15) to determine Im $M(O_s)$. Five seismogram sections for five different C, see Eq. (15), are shown: $C = 5, 2, 1, 0.5, 0.2$. The reduction velocity is 8 km/s

There are no sharp boundaries of shadow zones at $x = 500$ km and $x = 475$ km in the Gaussian beam synthetic seismograms. The wave field even penetrates into shadow zones. The maximum amplitudes of both reflected waves are shifted beyond the critical points, situated at $x = 385$ km and $x = 410$ km (see also Fig. 2). Thus, the Gaussian beam method eliminates certain singularities of the ray solutions in a qualitatively correct way.

The individual diagrams, for different C, differ in detail. For very large C, i.e. narrower Gaussian beams, the results are stable but closer to the ray solution. For very small C (see the diagram for $C = 0.2$), some weak spurious arrivals connected with strong refracted waves close to the source appear.

Option $C = 1$ yields very stable results; practically all spurious arrivals are suppressed. We cannot expect the accuracy to be optimum in this case, but the choice is a useful compromise. It yields results considerably more accurate than the ray method, both in situations which need very broad Gaussian beams and in situations which require narrow Gaussian beams.

The amplitudes of the refracted wave close to the source are not quite regular. The irregularities are caused by some small oscillations in the velocity gradient due to the application of the spline approximation. These oscillations are caused by the large gradients of velocity close to the Earth's surface. In Fig. 15a, we can see the ray diagram and the travel-time curve of the refracted wave close to the source. The ray diagram was computed by interval ray tracing. In the ray diagram, we can clearly see the effects of the slight variations in the velocity gradients. The density of rays is very high at $x = 340$ km and $x = 349$ km, which leads to larger amplitudes at these distances.

The Gaussian beam computation of synthetic seis-

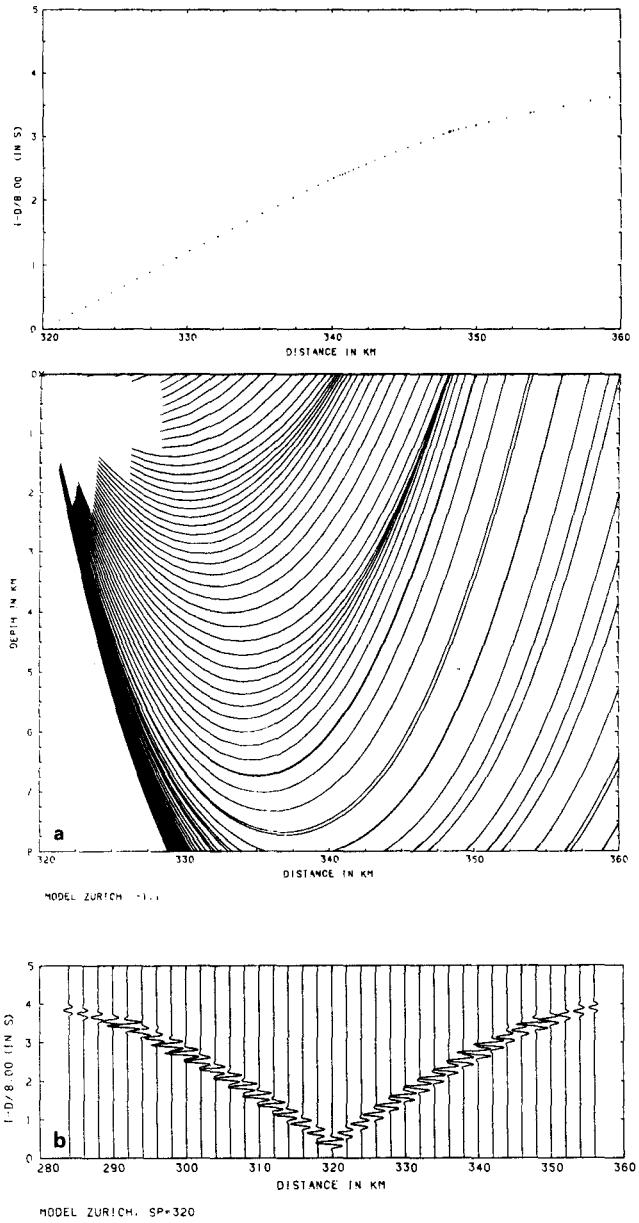

Fig. 15a and b. **a** Detailed ray diagram and the travel times of the P wave refracted in the immediate vicinity of the source, SP = 320 km, model Zurich (see Fig. 1). Two regions of increased density of rays are clearly seen; **b** Gaussian beam synthetic seismograms of the vertical component of the displacement vector of the P wave refracted in the immediate vicinity of the source, SP = 320 km, model Zurich (see Fig. 1). The parameters of Gaussian beams are chosen at the endpoints of rays, using Eq. (13) to determine $\mathrm{Re}\, M(O_s)$ and Eq. (14) to determine $\mathrm{Im}\, M(O_s)$

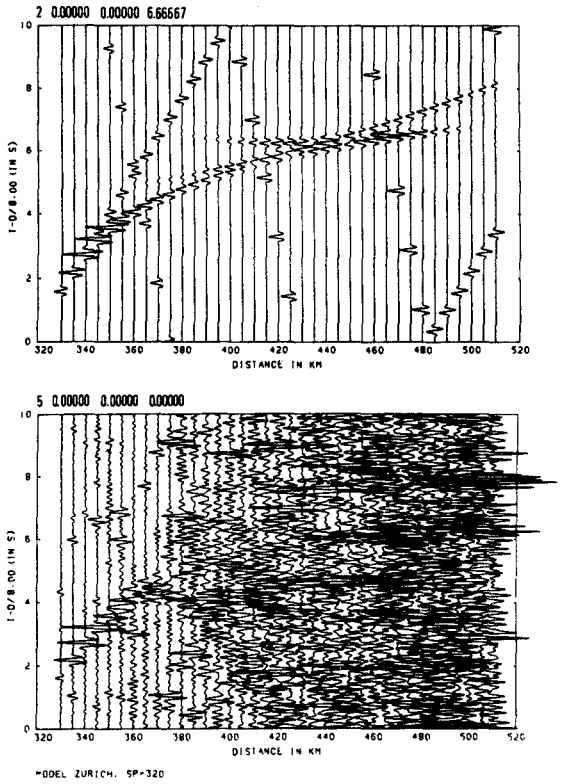

Fig. 16. Examples of choices of parameters of Gaussian beams leading to strong spurious arrivals and to instabilities. The same computation as in Fig. 14 only parameters of Gaussian beams are selected differently. In the *top diagram*, option (17) of very broad Gaussian beams is used. The broad Gaussian beams of strong refracted waves close to the source generate distinct spurious arrivals along the whole section. In the *bottom diagram*, the "true plane wave" option at the endpoints of rays is considered, $\mathrm{Re}\, M(O_s) = \mathrm{Im}\, M(O_s) = 0$ s/km^2

mograms is very stable even in the immediate vicinity of the source, if we use the choices of initial parameters of Gaussian beams suggested above. Figure 15b shows synthetic seismogram section evaluated in the immediate vicinity of the source. The section evaluated with $C = 1$ is again very stable.

Figure 16 shows two Gaussian beam synthetic seismogram sections with an improper choice of initial parameters of Gaussian beams. In the top diagram, option (17) of very broad Gaussian beams was used. This option yields excellent results in vertically inhomogeneous media, but may yield strong spurious arrivals in laterally varying structures, such as model Zurich. The Gaussian beams used for the computation are rather broad even in the vicinity of the source, where the refracted wave is very strong. These broad Gaussian beams contaminate the whole wave field, even at large epicentral distances. Strong spurious arrivals are obtained. The reverse branches of spurious arrivals are caused by the refracted wave propagating to the left of the shot point (due to the aliasing effect). It should be emphasized, however, that the actual synthetic seismograms (with spurious arrivals removed) look surprisingly good.

An extremely unstable choice of initial parameters of Gaussian beams is shown in the bottom diagram of Fig. 16. It corresponds to the *true plane wave option*, $\mathrm{Re}\, M(O_s) = \mathrm{Im}\, M(O_s) = 0$. Although the expansion into true plane waves is very useful in some simple types of media (homogeneous layers, plane interfaces), it is quite unsuitable in laterally varying complex layered structures.

Numerical example 8. Simple types of seismic sources

There are many possibilities of exploiting Gaussian beams in seismic source studies and in the evaluation of high-frequency strong-motion seismograms. Here we shall present the simplest possible alternative of Gaussian beam modelling of seismic sources in laterally varying media, based on a point source with non-symmetric radiation patterns. This possibility was included in program package BEAM 84. Some other possibilities, including sources of finite extent, will be shortly discussed later in this section. We shall discuss only 2-D media here. The generalization for 3-D media is, however, straightforward.

We shall consider the following three-types of radiation patterns:

a) *Isotropic source of the explosive type.* For P waves, the radiation pattern is isotropic (circular). No S waves are generated.

b) *Single force.* The direction of the force is specified by the angle φ, see Fig. 17. The radiation patterns for both P and S waves are two-lobed.

c) *Double couple without moment.* For the geometry of this source, see Fig. 18. The dip angle is denoted by δ. The radiation patterns for both P and S waves are four-lobed.

More details on radiation patterns and analytic expressions for them can be found in, e.g. Aki and Richards (1980), Kennett (1983).

We shall now present synthetic seismograms for the individual types of seismic sources described above. We shall again consider the model Zurich, $SP=320$ km. Interaction of the source with the Earth's surface is formally not considered. (It would, of course, be easy to include the interaction of the source with the surface in the computations.) Program package BEAM 84, described in the previous section, was used for the computations. Only P-wave synthetic seismograms will be presented here for simplicity. The evaluation of S waves, however, can also be performed optionally, together with the P waves or independently of them.

In all computations presented in this section, the parameters of Gaussian beams were specified at endpoints of rays, using Eqs. (13) and (15) with $C=1$. This choice of initial parameters guarantees stability of the computations, even in the case of stronger lateral variations of velocity close to the Earth's surface. The same file with the endpoint information was used as in example 7.

Synthetic seismograms for the isotropic source of P waves are shown in Fig. 19. The details of these seismograms were discussed in the previous section.

For a single force, see Fig. 20. In Fig. 20a, the vertical component synthetic seismograms for two inclination angles φ ($\varphi=0°$ and 90°) are shown. For comparison, Fig. 20b shows the horizontal synthetic seismograms for $\varphi=90°$.

Finally, synthetic seismograms for the double couple source are shown in Fig. 21. The four synthetic seismogram sections in Fig. 21 correspond to the dip angles 0°, 30°, 60° and 90°. In all cases, the vertical components of the displacement are shown. The differences between the individual synthetic sections are remarkable in this case. As we can see, the wave field

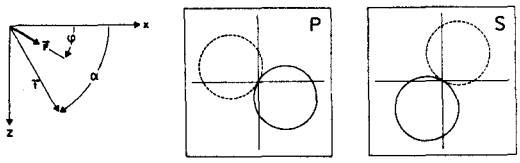

Fig. 17. Single-force radiation patterns. *Left:* The force is inclined by angle φ from the horizontal axis. *Right:* The single force radiation patterns of P and S waves for $\varphi=30°$. The *solid line* denotes positive values, *dashed line* negative values. $\vec{t}$ denotes the initial direction of the ray

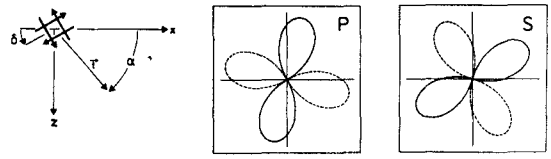

Fig. 18. Double couple radiation patterns. *Left:* Geometry of the source. *Right:* The double couple radiation patterns of P and S waves, $\delta=30°$. The *solid line* denotes positive values, the *dashed lines* negative values. $\vec{t}$ denotes the initial direction of the ray

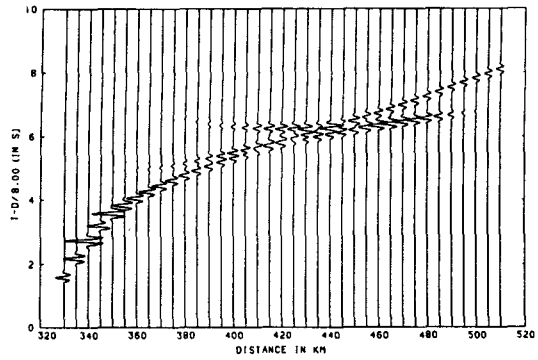

Fig. 19. Isotropic source of P waves. Gaussian beam synthetic seismograms of the vertical component of the displacement vector in model Zurich, SP = 320 km (see Fig. 1). The parameters of Gaussian beams are chosen at the endpoints of rays, using Eq. (13) to determine $\mathrm{Re}\,M(O_s)$ and Eq. (15) to determine $\mathrm{Im}\,M(O_s)$ (with $C=1$). The reduction velocity is 8 km/s

connected with deep discontinuities is considerably suppressed at larger epicentral distances for dip angles close to 30°. Distinct changes in the polarity of the individual waves can be observed in some diagrams. For example, see the synthetic section for the dip angle of 60°, in which the refracted wave in the first layer changes polarity at $x=345$ km.

It is obvious from the examples presented that the source mechanism has a strong influence on the observed high-frequency field. The application of the point source with a suitable radiation pattern, however, will often be too large a simplification of the actual situation; sources of finite extent must be considered. There are several possibilities of applying Gaussian beams in the numerical modelling of seismic wave fields

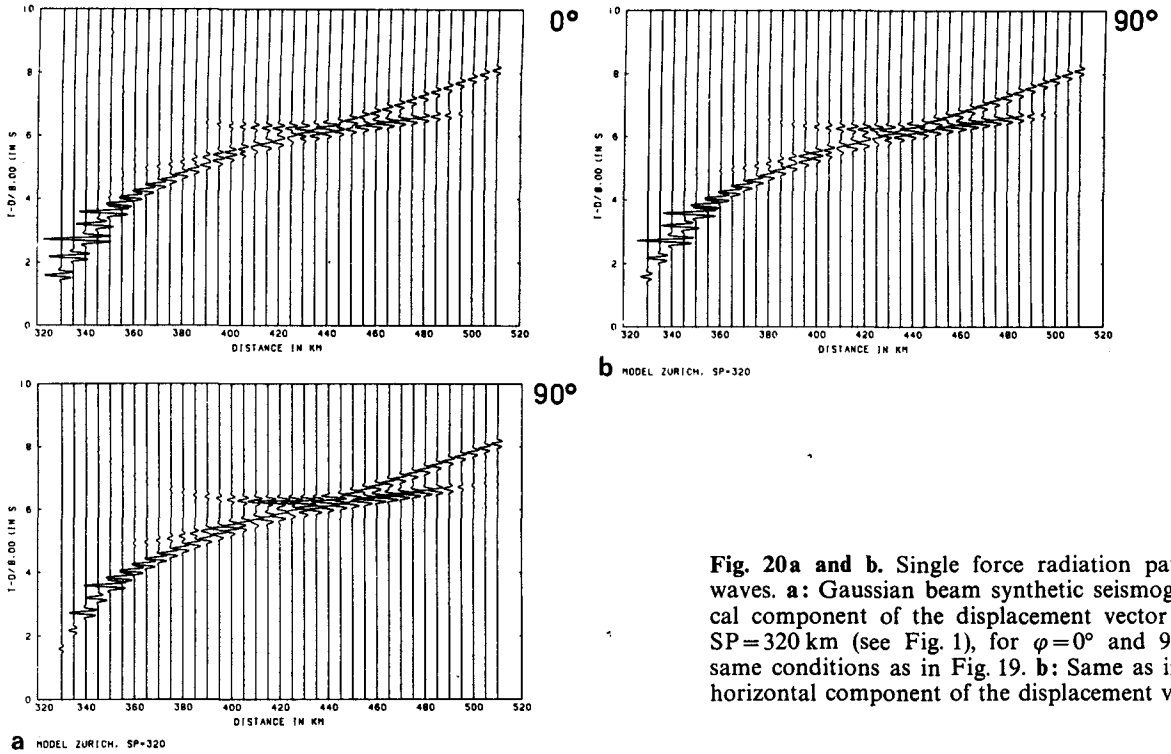

Fig. 20a and b. Single force radiation pattern source of *P* waves. **a:** Gaussian beam synthetic seismograms of the vertical component of the displacement vector in model Zurich, SP = 320 km (see Fig. 1), for $\varphi = 0°$ and 90°. Otherwise the same conditions as in Fig. 19. **b:** Same as in Fig. 20a, for the horizontal component of the displacement vector, $\varphi = 90°$

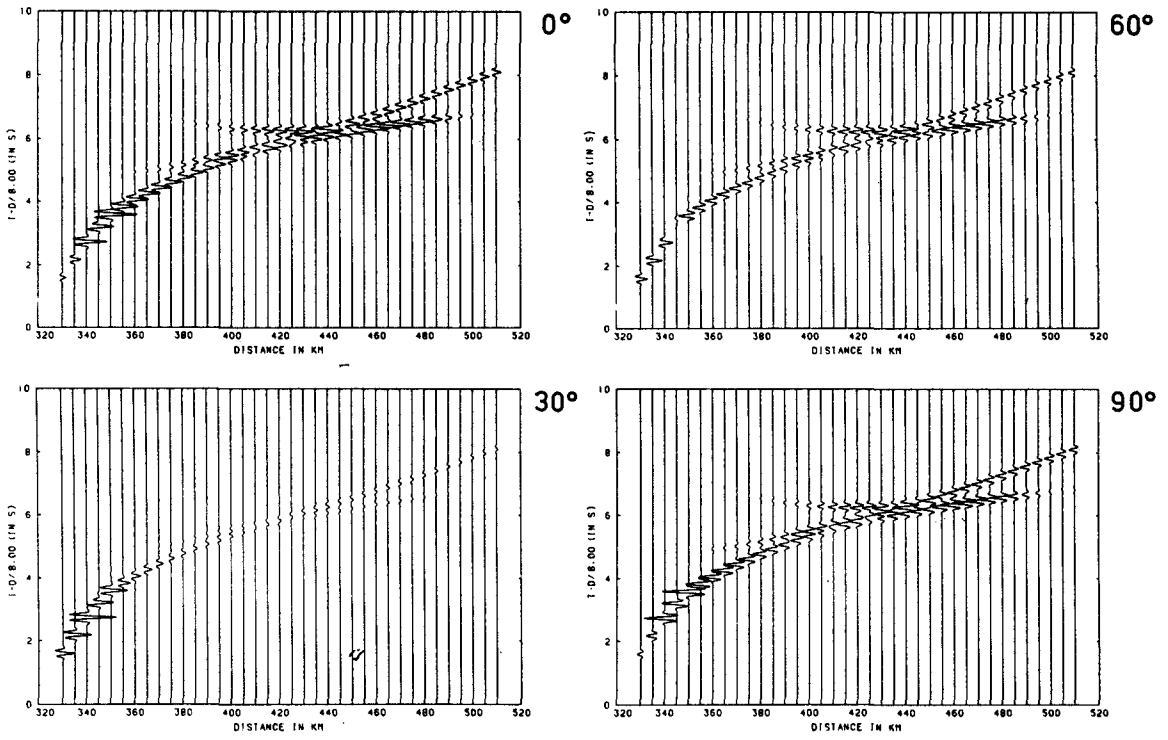

Fig. 21. Double couple radiation pattern source of *P* waves. Gaussian beam synthetic seismograms of the vertical component of the displacement vector in model Zurich, SP = 320 km (see Fig. 1), for $\delta = 0°$, 30°, 60° and 90°. Otherwise the same conditions as in Fig. 19

generated by sources of finite extent in complex structures. We shall mention three possibilities:

a) It would be possible to simulate the seismic source by a superposition of time-shifted point sources and to expand each point source into Gaussian beams. This would be a straightforward, but time-consuming approach.

b) Expansions of a wave field specified at an initial surface into Gaussian beams were found theoretically; for a scalar case by Klimeš (1984a) and for a vectorial

case by Červený (1985b). These expansions can be used in several ways. The first possibility is the direct expansion of the wave field along the fault plane into Gaussian beams. The second possibility is to use the finite differences to recalculate the wave field on some auxiliary surface surrounding the source and then expand the wave field at the surface into Gaussian beams.

c) Some new approaches, based on the isochron integration over the fault with the integrand containing a ray theoretical Green's function were proposed recently (see Madariaga, 1985; Bernard and Madariaga, 1984; Spudich and Frazer, 1984). The author believes that the application of Gaussian beams may be useful even in these approaches.

Numerical example 9. Slightly dissipative media

To perform computations of synthetic seismograms in laterally varying dissipative media is not a simple problem. Often, approximate approaches are used. In one of these approaches, we consider a complex-valued propagation velocity v_c with a small imaginary part, which is formally assumed to be of the order of ω^{-1} for $\omega \to \infty$ (the so-called Debye approximation). For details, see Kravtsov and Orlov (1980). The approach yields a new expression for the complex-valued travel time $\tau(O_s)$ in Eq. (5), $\tau(O_s) = \int_{O_0}^{O_s} [v_c(s)]^{-1}\, ds$. The integration is along the ray.

The method has justification only in slightly dissipative media. Under the above assumption, we can still consider seismic energy to propagate along the rays evaluated for a perfectly elastic medium. For a stronger absorption, however, a concept of complex rays should be used which would make the computations considerably more complicated.

In this section, we shall present an example of synthetic seismogram computations in slightly dissipative media. We again use model Zurich, $SP = 320$ km. The computations are performed by program package BEAM 84. Program package BEAM 84 includes, as a general possibility, Müller's absorption model with the power-law dependence of the quality factor Q on frequency,

$$Q(f) = Q(f_r)(f/f_r)^{\gamma}, \tag{19}$$

where γ is a constant, $-1 \leqq \gamma \leqq 1$, and f_r is a reference frequency for which $Q = Q(f_r)$ is known. See Müller (1983, 1985) where, also, relevant expressions for the phase velocity $v(f)$ and complex-valued velocity $v_c(f)$ can be found.

We now assume that the rays and travel times are calculated with the velocity $v(f_r)$, i.e. with the phase velocity corresponding to the reference frequency f_r. Then we introduce the quantity

$$t^* = \int_{O_0}^{O_s} [v(f_r)\, Q(f_r)]^{-1}\, ds,$$

where the integration is along the ray, from the source O_0 to the endpoint O_s. Using t^*, we can evaluate a frequency-dependent amplitude decay factor and include it in computations. For Müller's model, the amplitude decay factor $A_d(O_s)$ is as follows:

$$A_d(O_s) = \exp\left\{-\pi f t^* \left[(f_r/f)^{\gamma} \pm i \cot\left(\gamma \frac{\pi}{2}\right)(1-(f_r/f)^2)\right]\right\}. \tag{20}$$

The sign of the imaginary term in the exponent depends on the sign convention used in the Fourier transform. The same sign convention applies to Eqs. (21) and (22).

Even though program package BEAM 84 allows the general frequency dependence of Q given by Eq. (19) to be considered, we shall present computations only for $\gamma = 0$, for which the amplitude decay factor reduces to

$$A_d(O_s) = \exp\{-\pi f t^* \mp 2 i f t^* \ln(f/f_r)\}. \tag{21}$$

The second term in the exponential function represents a velocity dispersion correction which guarantees, approximately, the causality of results. If we take into account only the first term and neglect the second term in the exponential function, the causality is not guaranteed; we then speak of non-causal absorption.

For non-causal absorption, the factor $t^*/2$ can be included in the imaginary part of the complex-valued travel time and the Gaussian beam synthetic seismograms can be evaluated with the same speed as the synthetic seismograms for non-absorbing media. The second term in the exponential in Eq. (21) (the dispersion correction) is, unfortunately, non-linear in frequency f and would increase the computing time considerably. For slightly dissipative media, however, this term can be linearized. This linearization was proposed by Červený and Frangié (1980, 1982). The amplitude-decay factor, Eq. (21), then reads

$$A_d(O_s) = \exp\{-2\pi f[\tfrac{1}{2} t^* \pm i t^+] \pm 2 i f_M t^*\}. \tag{22}$$

Here f_M is the prevailing frequency of the signal under consideration, t^+ is given by the relation

$$t^+ = (t^*/\pi)[1 + \ln(f_M/f_r)]. \tag{23}$$

The linearized version of $A_d(O_s)$, Eq. (22), works especially well if the amplitude spectrum of the source-time function is very narrow and highly concentrated in the vicinity of the prevailing frequency f_M. This is the case for the Gaussian envelope signal, mainly for larger γ (say $\gamma > 3$). Moreover, in favour of the linearization, we can also point out that the instrument responses in seismology and seismic prospecting are usually narrow-banded.

Using the linearized form, Eq. (22), the term $\frac{1}{2} t^* \pm i t^+$ can again be included in the complex-valued travel time, and the remaining part, $\pm 2 i f_M t^*$, is independent of frequency and does not cause any difficulty. In this way, the synthetic seismograms can be computed with almost the same speed for the causal absorption as for the non-absorbing medium. To evaluate the frequency response, the fast frequency response algorithm (FFR) described by Červený (1985a) can again be used.

Four "Zurich" models, which differ only in the absorption parameters, are considered:

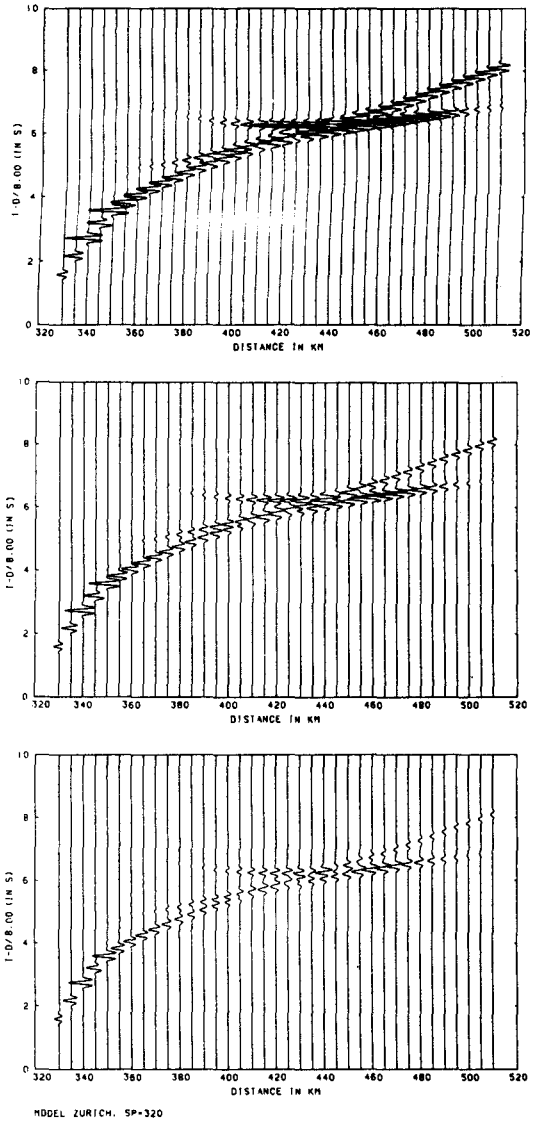

Fig. 22. Influence of absorption. Gaussian beam synthetic seismograms of the vertical component of the displacement vector in model Zurich, SP = 320 km (see Fig. 1). *Top diagram:* model without absorption. *Next two diagrams:* models with non-causal absorption. The absorption is larger in the *bottom diagram*, see text for details. The amplitude scaling factor is different from that in the other figures. Otherwise the same conditions as in Fig. 19

1) Model without absorption.

2) Model with non-causal absorption. The quality factors in the first and the third layer are $Q = 500$, and in the second layer, $Q = 700$.

3) Model with larger non-causal absorption. The quality factors are half of case 2.

4) Model with causal absorption. The quality factors are again half of case 2.

In Fig. 22, we can see three Gaussian beam synthetic seismogram sections, for models 1, 2 and 3 described above. (The results for the causal absorption will be shown later.) The same file with the endpoint information was used as in examples 7 and 8. The initial parameters of Gaussian beams were also selected in the same way as in examples 7 and 8. It was necessary to use different amplitude scalings, otherwise the amplitudes at larger epicentral distances would be too small in models 3 and 4. The amplitude scaling factor is $35(r/20)^{3/2}$. This amplitude scaling factor, of course, yields large amplitudes for the model without absorption, in comparison with previous computations; e.g., see Fig. 14. The non-causal absorption model used for the computations corresponds to Eq. (21) (Müller's model with Q independent of frequency) with the phase term neglected.

More detailed diagrams for one selected epicentral distance, $x = 470$ km, are shown in Fig. 23. The four columns correspond successively to the four models under consideration. In each column, the first diagram gives the frequency response, the second the spectrum of the synthetic seismogram and the third the synthetic seismogram. As the absorption increases, the amplitudes decrease (see the reduction factors shown above the diagrams), but the form of the signals changes only slightly. Certain small changes in the form of the signal can be observed in the case of causal absorption (see the last column). The linearized form of the amplitude decay factor, Eq. (22), was used to perform the causal absorption computations. The influence of absorption can clearly be observed in the diagrams of the frequency response.

Let us emphasize again that the evaluation of Gaussian beam synthetic seismograms for slightly dissipative media practically does not require more computer time than the evaluation of synthetic seismograms for non-dissipative media. The differences in the computer time were not measured during computations, but the author expects that they do not exceed 1% of the computer time, even for causal absorption (in a linearized form).

Other numerical tests and applications of the Gaussian beam summation method

The Gaussian beam summation method has recently been tested and applied to the solution of various problems of practical importance in seismology by several authors. In this section, we shall briefly list some results in this field. For more detailed conclusions, the reader is referred to the references.

Nowack and Aki (1984a) tested the 2-D Gaussian beam summation method using two approaches. One is the application of the reciprocity theorem for Green's function in arbitrary heterogeneous media. The second approach is to apply the Gaussian beam synthesis to cases for which solutions by other approximate methods are known. Let us name, among others, the soft-basin problem, which was attacked by several authors using the finite difference, finite element, discrete wavenumber and the glorified optics methods. It was found that the results were generally satisfactory. The Gaussian beam summation method was also used in two applications of practical importance in seismology: (a) to study volcanic earthquakes at Mt. St. Helens, (b) to study the scattering of teleseismic P waves by a lithosphere with randomly fluctuating velocities. The same authors, see Nowack and Aki (1984b), applied the Gaussian beam synthetic seismograms to the iterative inversion using complete waveforms.

Müller (1984) applied the Gaussian beam summation method to the computation of *SH* synthetic seismograms in 2-D smooth laterally varying media. He proposed subdividing the model into triangles with linear velocity and density laws. Although this approximation is not quite suitable in the case of ray synthetic seismogram computations due to fictitious interfaces of second-order, it is very useful and effective if the Gaussian beam method is applied. The results obtained in this way are quite stable and the computations are very fast. Müller tested the Gaussian beam method for vertically inhomogeneous media by comparison with the reflectivity method, and for laterally varying media by applying the reciprocity principle. He applied the method to the model of the crust-mantle transition with lateral heterogeneities. These complications were modelled, by and large, with success. The seismograms, however, depend to a certain extent on the choice of the beam parameters. The reciprocity principle yielded good agreement for slight lateral variations, but the difference increased with the strength of lateral heterogeneities.

The Gaussian beam summation method was applied to the computation of the wave field in waveguides by Katchalov and Popov (1981) and by Grikurov and Popov (1983a). An acoustic waveguide with a parabolic distribution of velocity is considered in the first paper and a surface waveguide in the second paper. The results obtained by the Gaussian beam summation method are compared with the exact solutions in the second paper. By comparison with the exact solution, it was shown that the method of Gaussian beams is effective for such computations. Its accuracy does not depend on the complications of the ray field (caustics, shadows). The accuracy of the method was lower at large distances from the source. These results are also discussed by Grikurov and Popov (1983b) and by Babich et al. (1984).

Madariaga (1984) studied the possibilities and limitations of the Gaussian beam summation method in the computation of synthetic seismograms for vertically inhomogeneous media. The choice of the parameters of Gaussian beams was studied in great detail. Proposals of suitable choices both for $\mathrm{Re}\, M$ and $\mathrm{Im}\, M$ were given (in a slightly different notation). It was found that high accuracy of the results is achieved mainly if very broad Gaussian beams are considered. Numerical examples proved that the Gaussian beam summation is a powerful tool for calculating synthetic seismograms in the presence of caustics, shadows or other singularities of the ray field. Compared to the WKBJ and Maslov methods, the method of Gaussian beam summation has the advantage that it is possible to control the amplitudes of the cutt-off phases due to the finite range of slowness integration. Moreover, one does not need to worry about weighting functions and p-caustics with the Gaussian beam method.

Madariaga and Papadimitriou (1985) presented a new formulation of the Gaussian beam summation method for the modelling of body phases in a spherically stratified elastic model of the Earth. They showed that the Gaussian beam method may be deduced from the plane wave decomposition of the field of a line or point source in an acoustic or elastic medium, when each plane wave is replaced by a slightly parabolic wave. The examples demonstrated the accuracy of the Gaussian beam summation in the modelling of upper mantle body phases. They also showed that the technique provides a simple, fast and accurate alternative to the generalized ray and reflectivity techniques. By applying Gaussian beams, a significant degree of freedom is gained which permits the number of rays in the expansion to be reduced, aliasing in the slowness domain to be eliminated and the truncation phases to be reduced.

Necessary and sufficient conditions for the existence of acoustic and seismic rays and beams in general inhomogeneous media without interfaces are investigated in detail by Ben-Menahem and Beydoun (1985a, b). These conditions are expressed in terms of new physical parameters: the threshold frequency associated with the P/S decoupling conditions, the cut-off frequency associated with the radiation zone condition, the total curvature of the wavefront and the Fresnel-zone radius. With the aid of the above parameters, simple validity conditions are obtained for the decoupled far-field, the decoupled near-field, two-point dynamic ray tracing, paraxial wave fields and Gaussian beams. Numerical examples for an explosive point source in a vertically inhomogeneous medium with a constant velocity gradient are presented and compared with exact solutions. Two examples show the application of the Gaussian beam method to different types of seismic problems: the vertical seismic profiling and shallow earthquake configurations.

Klimeš (1985) wrote a new, very general, program package SW 84 for the evaluation of Gaussian beam synthetic seismograms in 3-D laterally varying layered structures. The initial parameters of Gaussian beams can be selected in several ways, among others by minimizing the validity conditions 1 and 2 along the central ray. Ray, WKBJ and Maslov computations may also be performed by a proper choice of initial parameters of Gaussian beams. The steps in the ray parameters are automatically controlled to keep the discretization error under some limit. The program package is briefly described in Červený (1985a). One numerical example of computation of synthetic seismograms can also be found there. The program is especially efficient for the evaluation of synthetic seismograms for 3-D structures at receivers situated roughly along a straight line profile, if the epicentre is located close to the profile (so-called "profile mode" computation). The profile mode can also be efficiently used for synthetic vertical seismic profiling in 3-D structures; the profile corresponds to the borehole with the receivers and the source situated arbitrarily.

Fertig and Pšenčík (1985) discuss in detail the relations between the ray method, the paraxial approximation and the Gaussian beam method in the evaluation of synthetic seismograms. The main attention is devoted to the computational aspects.

Cormier and Spudich (1984) used the 2-D Gaussian beam summation method to calculate P-wave seismograms at ranges of less than 10 km for point sources located in a low-velocity wedge surrounding a fault. Synthetic calculations and data examples have demonstrated that a wedge-shaped zone of low velocity sur-

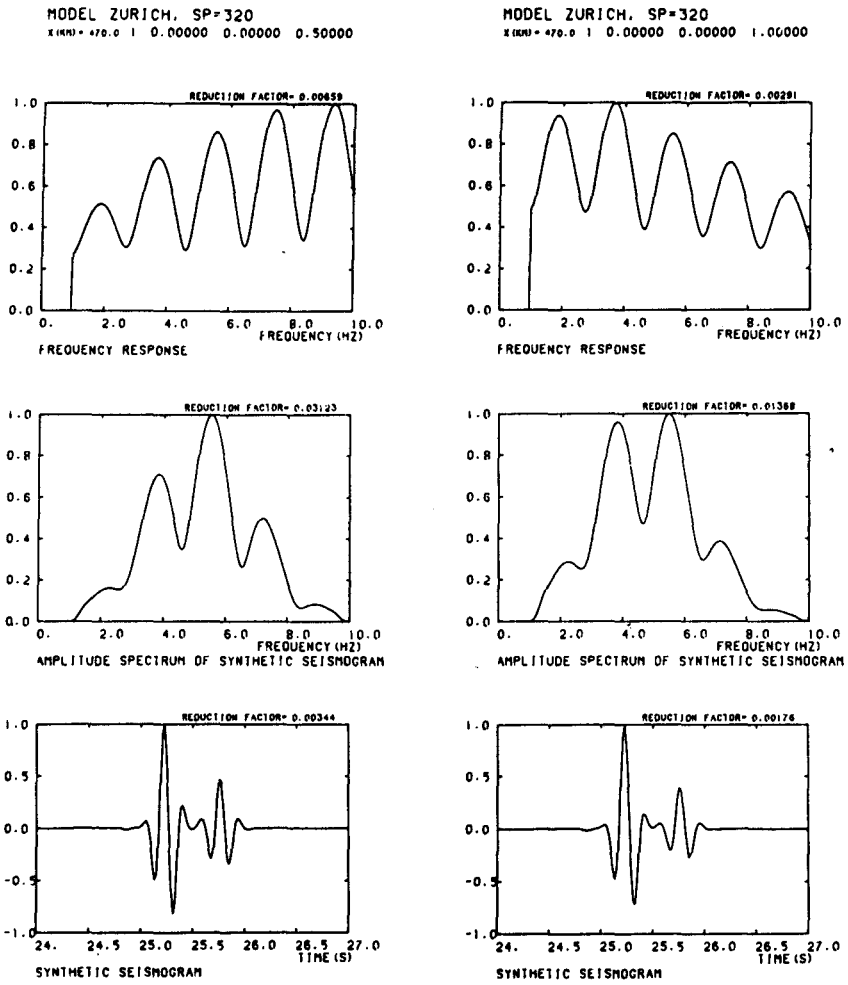

rounding a fault may account for the complexity and amplification of *P* waves from shallow focus events observed in the fault zone. Comparisons of Gaussian beam and *ART* synthetics were made for several wedge models discussed in the paper. Some difficulties of the Gaussian beam method, especially the lack of complete convergence of the Gaussian beam superposition in some situations, are discussed in detail.

Jobert and Jobert (1983) studied the propagation of a disturbance along the Earth's surface. Using the Gaussian beam computation scheme, rays were traced and synthetic seismograms obtained for a few spherical models with lateral inhomogeneities. In these results, deviations from the first-order perturbation theory for normal modes were displayed.

The Gaussian beams for surface waves in a medium, where the lateral variations of structure are very smooth were studied by Kirpichnikova (1971b) and by Yomogida (1985). In the frequency domain, see Yomogida (1985), the wave field is constructed from single mode surface waves which propagate along ray paths on the surface of the Earth, following the phase-velocity mapping for that frequency. The results of Yomogida (1985) were used by Yomogida and Aki (1985) in the total waveform synthesis of surface waves in a laterally heterogeneous Earth. A great advantage of surface-wave synthesis over body-wave synthesis is that for surface waves the problems are essentially two-dimensional (the rays are situated along the Earth's surface). The method of surface-wave synthesis by Gaussian beams differs from the body-wave synthesis in several ways, described in detail in the referred paper. Let us only mention that the speed of the wave packet along the ray is the local group velocity, even though the ray path itself is determined by the phase velocity. Yomogida and Aki found that the weighting functions of all Gaussian beams for a moment tensor representation of an earthquake are equivalent to those of far-field radiation patterns for a point double couple source. They also found that the choice of the initial parameters of Gaussian beams is not too critical for the results. The results of numerical tests for heterogeneous structure in the Pacific Ocean imply that the method may help to resolve small velocity anomalies, e.g. the hot spots such as the Hawaiian seamounts, or more precise lateral changes in seismic velocities near spreading ridges.

Alekseyev and Cheverda (1981) applied Gaussian beams to solve an important dynamic inverse problem of a laterally varying piece-wise homogeneous layered structure. They assumed that the wave field of a wave reflected from some curved interface, generated by a point source, was known in some finite region of the Earth's surface. They succeeded in determining not only the position and the geometrical shape in some "illumi-

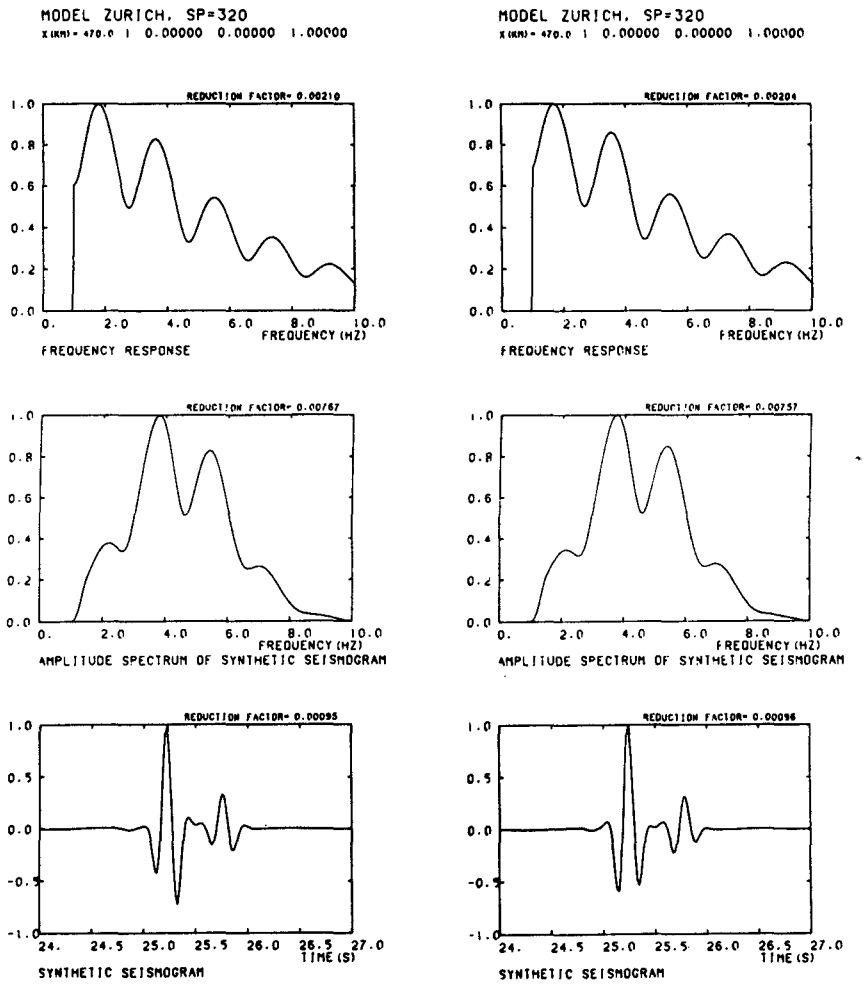

Fig. 23. Influence of absorption. Detailed pictures for the vertical component of the displacement vector in model Zurich, SP = 320 km, the receiver is situated at $x = 470$ km (epicentral distance equal to 160 km). The *first column* is for a non-absorbing medium, the *next two columns* for non-causal absorption (stronger in the latter case) and the *fourth column* for causal absorption. In each column, the *top diagram* is the frequency response, the *middle diagram* the amplitude spectrum of the synthetic seismogram and the *bottom diagram* the synthetic seismogram. The parameters of Gaussian beams were selected in the same way as in Fig. 19

nated" region of the interface, but also the reflection coefficients in that region of the interface. The authors suggest that an analogous approach can be developed to solve even more complex inverse dynamic structural problems.

Babich et al. (1984) reviewed the theory of Gaussian beams and of their summation. Several applications of the Gaussian beam summation method to waves propagating in waveguides are presented. Considerable attention is devoted to certain non-linear problems. Solutions of the non-linear Helmholtz equation (with the refractive index depending on the square of the amplitude of the wave field) concentrated close to rays are derived. The evolution of the wave packet in a non-linear inhomogeneous medium is studied.

Concluding remarks

In the conclusion of this paper we can say that the Gaussian beam summation method has, in general, yielded satisfactory results in the numerical modelling of high-frequency seismic wave fields in complex laterally varying layered structures and has found important applications in seismology and seismic prospecting.

Nevertheless, certain problems in the application of Gaussian beam summation are still open to further research. This applies mainly to the problem of the optimum choice of parameters of Gaussian beams, which would minimize the error of computations. It is obvious that this optimum choice will depend on the structure and velocity distribution along each ray under consideration (mainly on the velocity gradients). The author believes that some automatic optimum choices will be found in the near future.

We have discussed only the elastodynamic Gaussian beams in inhomogeneous elastic isotropic media. The elastodynamic Gaussian beams in pre-stressed anisotropic elastic media were investigated in detail by Hanyga (1985a, 1985b). The Gaussian beam approach can, however, be generalized even more; it can be applied to any wave field described by a system of linear partial differential equations of the second-order (see Nomofilov, 1981) and, perhaps, even to more complicated equations. The author believes that the Gaussian beams and Gaussian wave packets will find important applications even in some non-linear problems, both in the case of physical and geometrical non-linearities.

The main perspectives of the Gaussian beam summation approach consist in the solution of inverse dynamic seismic problems (using complete waveforms, amplitudes, amplitude ratios, spectral properties, etc.). The computed wave field is a linear superposition of Gaussian beams (or, in the time domain, of Gaussian envelope packets). The Gaussian beams and/or Gauss-

ian envelope packets are controlled by the velocity distribution only in some limited region; their properties do not depend on the whole structure. Thus, the application of Gaussian beams may be suitable to the investigation of localized velocity changes, geometrical and physical properties of seismic interfaces in some region, etc.

For the inversion of seismic data, it may be suitable to combine the Gaussian beam approach with the perturbation theory. Assume that the wave field in an unperturbed model D^0, generated by a point source situated at M^0, is evaluated at point M by the summation of Gaussian beams concentrated close to a two-parametric system of rays Ω^0. We would now like to evaluate the wave field at M in a perturbed model D. It would be necessary to evaluate a new system of rays Ω in D and evaluate the Gaussian beams concentrated close to these rays. The most time-consuming step in this procedure is the ray tracing of rays Ω. The procedure, however, can be simplified if the perturbation of the model is only slight, i.e. if model D is very close to the initial model D^0. It is then not necessary to evaluate the new system of rays Ω in the perturbed model D, but the Gaussian beams (or Gaussian wave packets) in the perturbed model D can be approximately evaluated using the old system of rays, Ω^0. This will save considerable computer time. The Gaussian beams, however, do not have their centre (maximum amplitudes) on the ray Ω^0 in this case, but the centre of the beam is laterally shifted outside Ω^0. A more detailed treatment of this problem will be published elsewhere.

The Gaussian beam with a lateral shift of its centre was investigated theoretically by Červený (unpublished manuscript). The equations which control the properties of such a beam were found. Such Gaussian beams may be important in the solution of some problems of seismological interest, e.g. in the more sophisticated investigation of overcritically reflected Gaussian beams and waves. The well-known lateral shift of the centre of the reflected beam is obtained which is closely connected with the changes of the argument of the complex-valued reflection coefficient. For $f \to \infty$, the lateral shift vanishes.

The Gaussian beam approach may find broad applications in many fields of seismology and of seismic prospecting. It can be used practically everywhere where the standard ray method is applicable. Certain such situations are listed in Červený (1985a). Let us note, among others, the applications to vertical seismic profiling, synthetic time-section calculations, strong-motion seismogram synthesis and interpretation, seismic tomography based on complete waveforms, borehole-to-borehole measurements. Gaussian wave packets have found applications even in such typical ray theory problems like the location of seismic sources. A new algorithm for the location of seismic sources in a 3-D complex structure, based on Gaussian wave packets, was proposed recently by Klimeš (unpublished manuscript, in Czech).

It is expected that the Gaussian beam summation method can be suitably combined with some other methods to produce even more powerful hybrid algorithms for the solution of both direct and inverse seismic problems, e.g. with the matrix reflectivity method, with the modal summation method and with the finite difference method. The hybrid reflectivity-Gaussian beam algorithm was programmed, tested and used to study the reflected *PP*, *PS*, *SP* and *SS* wave fields from thin transition layers by Černohlávková and Červený. The method is very efficient and is applicable even to *curved* thin transition layers. The detailed exposition will be published elsewhere.

The application of the Gaussian beam summation method is efficient both in 1-D media (vertically inhomogeneous, radially symmetric) and in 2-D and 3-D laterally varying layered structures. The computer time savings in comparison with some other, more accurate methods (finite differences, etc.) will, of course, be especially pronounced in the 3-D computations. Thus, the method has large potential, mainly in 3-D seismics.

Acknowledgements. Most of the results included in this paper were obtained by the author in close cooperation with Ivan Pšenčík and Luděk Klimeš. The author is very indebted to both of them. He also wishes to express his sincere thanks to Professor Jon Claerbout for his invitation to work for three months with the Stanford Exploration Project (1981), and to Professor Gerhard Müller for his invitation to work for three months (1984) with his group at the J.W. Goethe University, Frankfurt a.M. During the author's stay at Stanford, program package BEAM81 was written and numerical example 4 was computed. Similarly, during the author's stay at Frankfurt, the program package BEAM84 was finished and numerical examples 7, 8 and 9 were computed. He is also very grateful to Michael Weber and to the second anonymous reviewer for carefully reading this article and for numerous corrections, valuable comments and suggestions to it.

References

Aki, K., Richards, P.: Quantitative seismology. San Francisco: Freeman 1980

Alekseyev, A.S., Cheverda, V.A.: On an asymptotic method of the solution of a dynamic inverse problem of the theory of wave propagation in a piece-wise homogeneous layered structure (in Russian). Preprint No. 311. Novosibirsk: Computing Center, Acad. Sci. USSR (Siberian Branch) 1981

Arnaud, J.A., Kogelnik, H.: Gaussian light beams with general astigmatism. Applied Optics **8**, 1687–1693, 1969

Babich, V.M.: Eigenfunctions, concentrated in the vicinity of closed geodesics. In: Mathematical problems of the theory of propagation of waves (in Russian), Vol. 9, V.M. Babich, ed.: pp. 15–63. Leningrad: Nauka 1968

Babich, V.M., Buldyrev, N.J.: Asymptotic methods in problems of diffraction of short waves (in Russian). Moscow: Nauka 1972

Babich, V.M., Kirpichnikova, N.Y.: The boundary layer method in diffraction problems (in Russian). Leningrad: Leningrad University Press 1974 (English translation by Springer-Verlag, 1980)

Babich, V.M., Pankratova, T.F.: On discontinuities of the Green function of mixed problems for wave equation with variable coefficients. In: Problems of mathematical physics (in Russian), Vol. 6, V.M. Babich, ed.: pp. 9–27. Leningrad: Leningrad Univ. Press 1973

Babich, V.M., Popov, M.M.: Propagation of concentrated acoustical beams in three-dimensional inhomogeneous media (in Russian). Akust. Zh. **27**, 828–835, 1981

Babich, V.M., Ulin, V.V.: Complex-valued ray solutions and eigenfunctions, concentrated in the vicinity of a closed geodesic. In: Mathematical problems of the theory of

propagation of waves (in Russian), Vol. 11, V.M. Babich, ed.: pp. 6–13. Leningrad: Nauka 1981a

Babich, V.M., Ulin, V.V.: Complex space-time ray method and "quasiphotons". In: Mathematical problems of the theory of propagation of waves (in Russian), Vol. 12, V.M. Babich, ed.: pp. 5–12. Leningrad: Nauka 1981b

Babich, V.M., Molotkov, I.A., Popov, M.M.: Gaussian beams, concentrated close to lines of solution and their application (in Russian). Preprint No. 24 (396). Moscow: Inst. of Radioengineering and Electronics, Acad. Sci. USSR 1984

Ben Menahem, A., Beydoun, W.B.: Range of validity of seismic ray and beam methods in general inhomogeneous media. Part I: General theory. Geophys. J.R. Astron. Soc. 1985a (in press)

Ben Menahem, A., Beydoun, W.B.: Range of validity of seismic and beam methods in general inhomogeneous media. Part II: A canonical problem. Geophys. J.R. Astron. Soc. 1985b (in press)

Bernard, P., Madariaga, R.: A new asymptotic method for the modeling of near-field accelerograms. Bull. Seismol. Soc. Amer. **74**, 539–557, 1984

Černohlávková, D.: Seismic wave fields in simple structures (in Czech). Diploma Thesis. Prague: Charles University, Faculty of Mathematics and Physics 1985

Červený, V.: The amplitude-distance curves for waves reflected at a plane interface for different frequency ranges. Geophys. J.R. Astron. Soc. **13**, 187–196, 1967

Červený, V.: Seismic wave fields in structurally complicated media. Ray and Gaussian beam approaches. Lecture notes. Utrecht: Rijksuniversiteit Utrecht, Vening-Meinesz Laboratory 1981

Červený, V.: Expansion of a plane wave into Gaussian beams. Stud. Geophys. Geod. **26**, 120–131, 1982

Červený, V.: Synthetic body wave seismograms for laterally varying layered structures by the Gaussian beam method. Geophys. J.R. Astron. Soc. **73**, 389–426, 1983

Červený, V.: Ray synthetic seismograms for complex two-dimensional and three-dimensional structures. J. Geophys. **58**, 2–26, 1985a

Červený, V.: The application of ray tracing to the numerical modeling of seismic wavefields in complex structures. In: Seismic shear waves, G. Dohr, ed.: pp. 1–124. Handbook of geophysical exploration, Section I: Seismic exploration, K. Helbig and S. Treitel, eds. London: Geophysical Press 1985b

Červený, V., Frangié, A.B.: Elementary seismograms of seismic body waves in dissipative media. Stud. Geophys. Geod. **24**, 365–372, 1980

Červený, V., Frangié, A.B.: Effects of causal absorption on seismic body waves. Stud. Geophys. Geod. **26**, 238–253, 1982

Červený, V., Janský, J.: Fast computation of ray synthetic seismograms in vertically inhomogeneous media. Stud. Geophys. Geod. **29**, 49–67, 1985a

Červený, V., Janský, J.: Fast computation of seismic wave fields in inhomogeneous media. In: Methods of processing of seismic reflection and refraction data (in Czech), M. Fejfar, ed. Brno: Geofyzika N.E., 1985b (in press)

Červený, V., Klimeš, L.: Synthetic body wave seismograms for three-dimensional laterally varying media. Geophys. J.R. Astron. Soc. **79**, 119–133, 1984

Červený, V., Pšenčík, I.: Gaussian beams in two-dimensional elastic inhomogeneous media. Geophys. J.R. Astron. Soc. **72**, 417–433, 1983a

Červený, V., Pšenčík, I.: Gaussian beams and paraxial ray approximation in three-dimensional elastic inhomogeneous media. J. Geophys. **53**, 1–15, 1983b

Červený, V., Pšenčík, I.: Gaussian beams in two-dimensional laterally varying layered structures. Geophys. J.R. Astron. Soc. **78**, 65–91, 1984

Červený, V., Popov, M.M., Pšenčík, I.: Computation of wave fields in inhomogeneous media – Gaussian beam approach. Geophys. J.R. Astron. Soc. **70**, 109–128, 1982

Chapman, C.H.: A new method for computing synthetic seismograms. Geophys. J.R. Astron. Soc. **54**, 481–518, 1978

Chapman, C.H.: Ray theory and its extensions-WKBJ and Maslov seismograms. J. Geophys. **58**, 27–43, 1985

Chapman, C.H., Drummond, R.: Body wave seismograms in inhomogeneous media using Maslov asymptotic theory. Bull. Seismol. Soc. Amer. **72**, S277–S317, 1982

Claerbout, J.F.: Fundamentals of geophysical data processing. New York: McGraw-Hill 1976

Cormier, V.F., Spudich, P.: Amplification of ground motion and wavefront complexity in fault zones; examples from the San Andreas and Calaveras Faults. Geophys. J.R. Astron. Soc. **79**, 135–152, 1984

Deschamps, G.A.: The Gaussian beams as a bundle of complex rays. Electr. Lett. **7**, 684–685, 1971

Felsen, L.B.: Evanescent waves. J. Opt. Soc. Amer. **66**, 751–760, 1976a

Felsen, L.B.: Complex-source-point solutions of the field equations and their relation to the propagation and scattering of Gaussian beams. Inst. Naz. Alta Matem., Symp. Math. **18**, 39–56, 1976b

Felsen, L.B.: Geometrical theory of diffraction, evanescent waves, complex rays and Gaussian beams. Geophys. J.R. Astron. Soc. 1985 (in press)

Felsen, L.B., Marcuvitz, N.: Radiation and scattering of waves. Englewood Cliffs: Prentice Hall 1973

Fertig, J., Pšenčík, I.: Numerical modeling of *P* and *S* waves in explosion seismology. In: Seismic shear waves, G. Dohr, ed. Handbook of geophysical exploration, Section I: Seismic exploration, K. Helbig and S. Treitel, eds. London: Geophysical Press 1985

Fock, V.A.: Electromagnetic diffraction and propagation problems. New York: Pergamon Press 1965

Frazer, L.N.: Feynman path integral synthetic seismograms. Trans. Amer. Geophys. Un. **64**, 772, 1983

Frazer, L.N.: Reflection seismograms using multi-fold path integrals. Geophys. J.R. Astron. Soc. 1985 (in press)

Frazer, L.N., Sen, K.M.: Kirchhoff-Helmholtz reflection seismograms in a laterally inhomogeneous multi-layered elastic medium, Part I: Theory. Geophys. J.R. Astron. Soc. **80**, 121–147, 1985

Grikurov, V.E., Popov, M.M.: Summation of Gaussian beams in a surface waveguide. Wave Motion **5**, 225–233, 1983a

Grikurov, V.E., Popov, M.M.: On the computation of waveguides by the method of summation of Gaussian beams (in Russian). Izv. Acad. Sci. USSR, Physics of the Earth No. 8, 101–103, 1983b

Haines, A.J.: A phase-front method I: Narrow-frequency-band *SH* waves. Geophys. J.R. Astron. Soc. **72**, 783–808, 1983

Haines, A.J.: A phase-front method II: Broad-frequency-band *SH* waves. Geophys. J.R. Astron. Soc. **77**, 43–64, 1984a

Haines, A.J.: A phase-front method III: Acoustic waves, *P*- and *S*-waves. Geophys. J.R. Astron. Soc. **77**, 65–104, 1984b

Hanyga, A.: Gaussian beams in anisotropic elastic media. Geophys. J.R. Astron. Soc. 1985a (in press)

Hanyga, A.: Gaussian beams in anisotropic elastic media and applications. In: Proceedings of the workshop on hybrid formulation of wave propagation and scattering, L.B. Felsen, ed. Amsterdam: Martinus Nijhoff 1985b (in press)

Hönl, H., Maue, A.W., Westphal, K.: Theorie der Beugung. Berlin-Göttingen-Heidelberg: Springer Verlag 1961

Hudson, J.A.: A parabolic approximation for elastic waves. Wave Motion **2**, 207–214, 1980

Jobert, N., Jobert, G.: An application of ray theory to the propagation of waves along a laterally heterogeneous spherical surface. Geophys. Res. Lett. **10**, 1148–1151, 1983

Katchalov, A.P.: Coordinate system for description of the "quasiphoton". In: Mathematical problems of the theory of propagation of waves (in Russian), Vol. 14, V.M. Babich, ed.: pp. 73–76. Leningrad: Nauka 1984

Katchalov, A.P., Popov, M.M.: The application of the Gaussian beam summation method to the computation of wave fields in the high-frequency approximation. Dokl. Akad. Nauk SSSR **258(5)**, 1097–1100, 1981

Katchalov, A.P., Popov, M.M., Pšenčík, I.: On the application of the method of summation of Gaussian beams to the problems of boundaries with edges. In: Mathematical problems of the theory of propagation of waves (in Russian), Vol. 13, V.M. Babich, ed.: pp. 65–71. Leningrad: Nauka 1983

Keller, J.B., Streifer, W.: Complex rays with an application to Gaussian beams. J. Opt. Soc. Amer. **61**, 40–43, 1971

Kennett, B.L.N.: Seismic wave propagation in stratified media. Cambridge: Cambridge Univ. Press 1983

Kirpichnikova, N.J.: Construction of solutions concentrated close to rays for the equations of elasticity in an inhomogeneous isotropic space. In: Mathematical problems of theory of diffraction and propagation of waves (in Russian), Vol. 1, V.M. Babich, ed.: pp. 103–113. Leningrad: Nauka 1971a (English translation by American Mathematical Society, 1974)

Kirpichnikova, N.J.: On the propagation of surface waves concentrated close to rays in an inhomogeneous elastic body of an arbitrary form. In: Mathematical problems of theory of diffraction and propagation of waves (in Russian), Vol. 1, V.M. Babich, ed.: pp. 114–130. Leningrad: Nauka 1971b

Klimeš, L.: Hermite-Gaussian beams in inhomogeneous elastic media. Stud. Geophys. Geod. **27**, 354–365, 1983

Klimeš, L.: Expansion of a high-frequency time-harmonic wavefield given on an initial surface into Gaussian beams. Geophys. J.R. Astron. Soc. **79**, 105–118, 1984a

Klimeš, L.: The relation between Gaussian beams and Maslov asymptotic theory. Stud. Geophys. Geod. **28**, 237–247, 1984b

Klimeš, L.: Computation of seismic wave fields in 3-D media by the Gaussian beam method. Program package SW 84 (in Czech). Research Report No. 68. Prague: Charles University, Institute of Geophysics 1985

Konopásková, J., Červený, V.: Numerical modelling of time-harmonic seismic wave fields in simple structures. Part I: Stud. Geophys. Geod. **28**, 19–35, 1984. Part II: Stud. Geophys. Geod. **28**, 113–128, 1984

Kravtsov, Yu.A., Orlov, Yu.I.: Geometrical optics of inhomogeneous media (in Russian). Moscow: Nauka 1980

Landers, T., Claerbout, J.F.: Numerical calculation of elastic waves in laterally inhomogeneous media. J. Geophys. Res. **77**, 1476–1482, 1972

Leontovich, M.A., Fock, V.A.: Solution of the problem of propagation of electromagnetic waves along the Earth's surface using the parabolic equation method (in Russian). ZETF **16**, 557–573, 1946

Madariaga, R.: Gaussian beam synthetic seismograms in a vertically varying medium. Geophys. J.R. Astron. Soc. **79**, 589–612, 1984

Madariaga, R., Bernard, P.: Ray theoretical strong motion synthesis. J. Geophys. **58**, 73–81, 1985

Madariaga, R., Papadimitriou, P.: Gaussian beam modelling of upper mantle phases. Ann. Geophys. 1985 (in press)

Maslov, V.P.: Complex method WKB in non-linear equations (in Russian). Moscow: Nauka 1977

McCoy, J.J.: A parabolic theory of stress wave propagation through inhomogeneous linearly elastic solids. J. Appl. Mech. **44**, 462–482, 1977

Müller, G.: Rheological properties and velocity dispersion of a medium with power-low dependence of Q on frequency. J. Geophys. **54**, 20–29, 1983

Müller, G.: Efficient calculation of Gaussian beam seismograms for two-dimensional inhomogeneous media. Geophys. J.R. Astron. Soc. **79**, 153–166, 1984

Müller, G.: The reflectivity method: a tutorial. J. Geophys. **58**, 153–174, 1985

Nomofilov, V.E.: Asymptotic solutions of a system of differential equations of the second order, concentrated close to a ray. In: Mathematical problems of the theory of propagation of waves (in Russian), Vol. 11, V.M. Babich, ed.: pp. 170–179. Leningrad: Nauka 1981

Nowack, R., Aki, K.: The 2-D Gaussian beam synthetic method: testing and applications. J. Geophys. Res. **89**, 1466–1494, 1984a (chybná citace)

Nowack, R., Aki, K.: Iterative inversion for structure using complete waveforms (abstract). EOS Trans. AGU **65**, 237, 1984b

Popov, M.M.: A new method of computation of wave fields using Gaussian beams. Wave Motion **4**, 85–95, 1982

Ru-Shan Wu: Analytic extension of Green's function, complex rays and Gaussian beams in smoothly inhomogeneous media. Geophys. J.R. Astron. Soc. 1985 (in press)

Scott, P., Helmberger, D.H.: Applications of the Kirchhoff-Helmholtz integral to problems in seismology. Geophys. J.R. Astron. Soc. **72**, 237–254, 1983

Sen, M.K., Frazer, L.N.: Kirchhoff-Helmholtz reflection seismograms in a laterally inhomogeneous multi-layered elastic medium, Part II: Computations. Geophys. J.R. Astron. Soc. 1985 (in press)

Sinton, J.B., Frazer, L.N.: Using Kirchhoff's method to compute finite-frequency body wave synthetic seismograms in laterally varying media. Trans. Amer. Geophys. Un. **62**, 956, 1981

Sinton, J.B., Frazer, L.N.: A Kirchhoff method for the computation of finite frequency body wave synthetic seismograms in laterally varying media. Geophys. J.R. Astron. Soc. **71**, 37–55, 1982

Spudich, P., Frazer, L.N.: Use of ray theory to calculate high-frequency radiation from earthquake sources having spatially variable rupture velocity and stress drop. Bull. Seismol. Soc. Amer. **74**, 2061–2082, 1984

Sutton, G.R.: The effect of velocity variations on the beam width of seismic wave. Geophysics **49**, 1649–1652, 1984

Tappert, F.D.: The parabolic approximation method. In: Wave propagation and underwater acoustics. Lecture Notes in Physics, Vol. 70, J.B. Keller and J.S. Papadakis, eds.: pp. 224–287. Berlin: Springer-Verlag 1977

Yomogida, K.: Gaussian beams for surface waves in laterally slowly varying media. Geophys. J.R. Astron. Soc. 1985 (in press)

Yomogida, K., Aki, K.: Waveform synthesis of surface waves in a laterally heterogeneous Earth by the Gaussian beam method. J. Geophys. Res. 1985 (in press)

Received February 5, 1985; revised version May 2, 1985
Accepted May 3, 1985